DECEMBER 2025 M.Sc. in Civil Engineering OSAMA RAHIM SHIKH HASAN

REPUBLIC OF TÜRKİYE
GAZİANTEP UNIVERSITY
GRADUATE SCHOOL OF NATURAL & APPLIED SCIENCES

# NUMERICAL MODELING OF LOCAL SCOUR AROUND CIRCULAR BRIDGE PIERS ARRANGED IN A TRIANGULAR CONFIGURATION

**M.Sc. THESIS**
**IN**
**CIVIL ENGINEERING**

BY
OSAMA RAHIM SHIKH HASAN
DECEMBER 2025

# NUMERICAL MODELING OF LOCAL SCOUR AROUND CIRCULAR BRIDGE PIERS ARRANGED IN A TRIANGULAR CONFIGURATION

**M.Sc. Thesis**

**in**

**Civil Engineering**

**Gaziantep University**

**Supervisor**

**Prof. Dr. Mustafa GÜNAL**

**by**

**Osama RAHIM SHIKH HASAN**

**December 2025**

**NUMERICAL MODELING OF LOCAL SCOUR AROUND CIRCULAR BRIDGE PIERS ARRANGED IN A TRIANGULAR CONFIGURATION**

submitted by **Osama RAHIM SHIKH HASAN** in partial fulfillment of the requirements for the degree of Master of Science in **Civil Engineering, Gaziantep University** is approved by,

Prof. Dr. Ahmet Necmeddin YAZICI
Director of the Graduate School of Natural and Applied Sciences ………..............

Prof. Dr. Nildem TAYŞİ
Head of the Department of Civil Engineering ………..............

Prof. Dr. Mustafa GÜNAL
Supervisor, Civil Engineering
Gaziantep University ………..............

Exam Date: 05.December.2025

**Examining Committee Members:**

Prof. Dr. Mustafa GÜNAL
Gaziantep University ………..............

Asst. Prof. Dr. Ayşe Yeter GÜNAL
Gaziantep University ………..............

Assist. Prof. Dr. Osman HANSU
Gaziantep Islam Science and Technology University ………..............

**I hereby declare that all information in this document has been obtained and presented in accordance with academic rules and ethical conduct. I also declare that, as required by these rules and conduct, I have fully cited and referenced all material and results that are not original to this work.**

**Osama RAHIM SHIKH HASAN**

# ABSTRACT

## NUMERICAL MODELING OF LOCAL SCOUR AROUND CIRCULAR BRIDGE PIERS ARRANGED IN A TRIANGULAR CONFIGURATION

**RAHIM SHIKH HASAN, Osama**
**M.Sc. in Civil Engineering**
**Supervisor: Prof. Dr. Mustafa GÜNAL**
**December2025**
**69 pages**

Bridge piers are essential structural elements that support bridges over water bodies. however, their exposure to hydrodynamic forces makes them exposed to local scour and corrosion. local scour, caused by the removal of sediment around bridge piers due to water flow, weakens the foundation and can lead to structural instability. understanding the interaction between hydrodynamic forces, scour mechanisms, and corrosion effects is crucial for designing durable bridge foundations. This study aims to investigate the local scour around a triangular group of circular bridge piers. by simulating (flow field, sediment transport, and corrosion processes) the study will provide evaluating the effects of local scour on the stability of circular bridge piers in a triangular configuration also, to give an insight into the mechanisms affecting bridge pier stability. Additionally, to propose effective mitigation strategies. This study will contribute to the field of hydraulic engineering by providing a detailed analysis of scouring processes using FLOW-3D software. The findings will help in designing more resilient bridge foundations and reduce potential failures due to hydrodynamic forces and material degradation.



**Key Words:** Local scour, Bridge piers, Numerical modeling, FLOW-3D, Hydrodynamic forces

# ÖZET

## ÜÇGEN DÜZENDE YERLEŞTİRİLMİŞ DAİRESEL KÖPRÜ AYAKLARI ETRAFINDA OLUŞAN YEREL OYULMANIN SAYISAL MODELLEMESİ

**RAHIM SHIKH HASAN, Osama**
**Yüksek Lisans Tezi, İnşaat Mühendisliği**
**Danışman: Prof. Dr. Mustafa GÜNAL**
**Aralık 2025**
**69 sayfa**

Köprü ayakları, su kütleleri üzerindeki köprüleri taşıyan temel yapısal elemanlardır. Ancak bu ayaklar, akışkan kuvvetlere maruz kaldıklarından, yerel aşınma ve korozyon etkilerine karşı hassastır. Akışın etkisiyle köprü ayakları çevresindeki zemin malzemesinin uzaklaşması sonucu meydana gelen yerel aşınma, temeli zayıflatmakta ve yapısal kararsızlığa yol açabilmektedir. Bu nedenle, hidrodinamik kuvvetler, aşınma mekanizmaları ve korozyon etkileri arasındaki etkileşimin anlaşılması, dayanıklı ve uzun ömürlü köprü temellerinin tasarımı açısından büyük önem taşımaktadır. Bu çalışma, üçgen biçiminde düzenlenmiş dairesel köprü ayakları etrafındaki yerel aşınmanın sayısal olarak incelenmesini amaçlamaktadır. Akış alanı, malzeme taşınımı ve korozyon süreçleri sayısal olarak modellenerek, üçgen konfigürasyondaki köprü ayaklarının stabilitesi üzerindeki yerel aşınma etkileri değerlendirilecektir. Ayrıca çalışma, köprü ayağı stabilitesini etkileyen mekanizmalar hakkında ayrıntılı bir anlayış sunmayı ve etkili aşınma önleme stratejileri önermeyi hedeflemektedir. Sayısal simülasyonlar, karmaşık hidrolik ve sediman taşınımı süreçlerini detaylı bir şekilde analiz etmeye olanak sağlayan FLOW-3D yazılımı kullanılarak gerçekleştirilmiştir. Bu araştırmadan elde edilecek bulguların, hidrolik mühendisliği alanına katkı sağlayarak yerel aşınma süreçlerinin daha iyi anlaşılmasına ve hidrodinamik kuvvetler ile malzeme bozulmasından kaynaklanan yapısal arızaların azaltılmasına yönelik daha dayanıklı köprü temellerinin tasarlanmasına yardımcı olması beklenmektedir.



**Anahtar Kelimeler:** Yerel oyulma, Köprü ayakları, Sayısal modelleme, FLOW-3D, Hidrodinamik kuvvetler.

*''Dedicated to my family''*

## ACKNOWLEDGEMENTS

I would like to thank my supervisor, Prof. Dr. Mustafa GÜNAL for his guidance and support throughout the study. I am thankful for his continued encouragement, motivation and invaluable support throughout the course of this research. His insightful feedback, patience and motivation have greatly contributed to the success of this work and to my academic development.

I am also sincerely thankful to all members of the Civil Engineering Department for their cooperation, helpful discussion and for providing a supportive and inspiring research environment.

My heartful appreciations go to my beloved family, whose unconditional love, patience, and encouragement have been my greatest source of strength. Their faith in me has always inspired me to overcome challenges and continue moving forward.

This work is dedicated to you—my mom, dad, wife, children, brothers, and friends. Thank you all for being part of this journey.

## TABLE OF CONTENTS

## LIST OF TABLES

**Page**

## LIST OF FIGURES

**Page***

.

## LIST OF SYMBOLS

| | | |
|---|---|---|
| **A** | Flow cross-sectional area | $m^2$ |
| **B** | Width of the flume | m |
| **D** | Flow depth | m |
| **$D_{50}$** | Median sediment size | mm / m |
| **D** | Pier diameter | m |
| **Fr** | Froude number | (dimensionless) |
| **G** | Gravitational acceleration | $m/s^2$ |
| **Q** | Discharge | $m^3/s$ |
| **Re** | Reynolds number | (dimensionless) |
| **T** | Time | secund/ Minutes |
| **U** | Velocity | m/s |
| **U*** | Shear velocity | m/s |
| **V** | Average velocity | m/s |
| **X, Y, Z** | Cartesian coordinates | m |
| **P** | Fluid density | $kg/m^3$ |
| **$\tau$** | Shear stress | $N/m^2$ |

# CHAPTER 1
# INTRODUCTION

## 1.1 Motivation of Study

Bridges are one of the most important components of infrastructure because these structures connect transportation networks and provide everyday transportation. However, the possibility of these buildings to collapse, whether partial or entirety, remains as a considerable hazard. Among the hydraulic factors that contribute to the erosion or weakening of riverine structures, the phenomenon of local scour stands out as one of the most critical and dangerous, given its direct impact on undermining foundations.

This phenomenon happens, when water flows within the waterway considered as main reason for sediment transportation from the bed of river which causes the continue changes in the elevation of the bed-river over the waterway, this problem increasing as of the humane intervention like construction bridges on the rivers which causing reducing the river cross section that lead to increase the water flow velocity, the sediment transportation also increasing in the flow turbulence and creating downward vortexes started in the front face and continue to the bottom of the bridge elements like piers and abutments, which eventually forming scour hole  around bridge pier foundations.  As shown in the Figure 1.1.

**Figure 1. 1** Scour hole around bridge pier (Melville & Coleman, 2000).

The breakdown of bridge failure causes from 2009 to 2018 is shown as in Figure 1.2 follows: (a) the percentage share of each cause of collapse, and (b) how much of these failures were due to natural causes versus human-related factors.

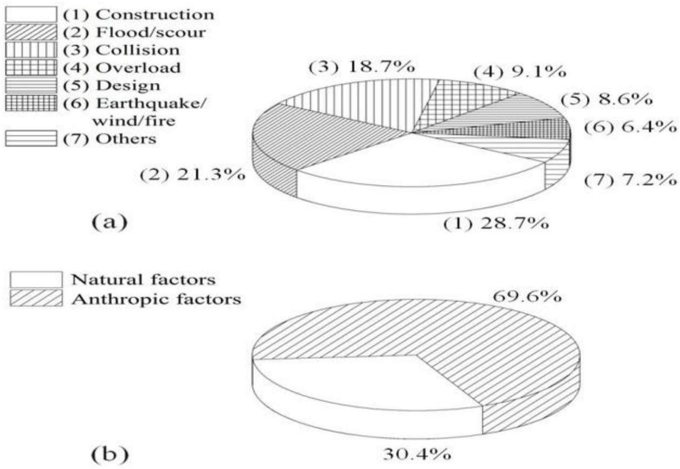


**Figure 1. 2** Bridge failure causes from 2009 to18 (Tan et al., 2020)

Also, It has been reported by A previously research by  Maddison (2012); Pagán-Ortiz (2002); Wang, Yu, et al. (2017); Zhang et al. (2022) showed that scour is one of the leading causes of bridge failure, with around 60% of bridge collapses in the United States since 1950 attributed to scour effects. According to reports from the Federal Highway Administration (FHWA), local scour has caused the collapse of more than 600 bridges in the U.S. in recent decades, underscoring the danger of this phenomenon and the need for scientific and engineering intervention. According to Lagasse et al., the failure of approximately 488,750 bridges in the United States has been linked to scour around pier foundations, resulting in annual economic losses estimated at around $30 million. One of the most tragic examples of bridge failure caused by excessive scour beneath pile foundations is the collapse of the Schoharie Creek Bridge on the New York State Thruway, which occurred on April 5, 1987. As illustrated in Figure 1.3, this incident led to five vehicles plunging into the river, making it one of the deadliest bridge collapse events in U.S. history.

**Figure 1.3** Eastbound view of the New York State Thruway bridge collapse over the Schoharie Creek on April 5, 1987.

Scouring commonly develops around bridge abutments and piers, posing a serious threat to the structural integrity of the bridge. This phenomenon occurs due to the disruption of natural river flow caused by the presence of these structural elements in the water. The velocity and pressure distribution surrounding a group of piers changes, strengthening vortex formation and increasing scour intensity as compared to single piers. the geometric arrangement of piers (such as the triangular arrangement) significantly affects the location and severity of scour due to the complex interactions between flow currents and the vortices generated by each individual pier, as well as the interactions between them (Akhlaghi et al., 2020; Heidarpour et al., 2010; Wang, Liang, et al., 2017).

Therefore, studying the behaviour of local scour around a triangular group arrangement of circular piers is of considerable importance, as a triangular group arrangement of circular piers form is commonly used in modern bridge pier designs and may lead to more complex and severe scour behaviour than traditional cases if it included error or insufficient research in design stage. This study depending on previous research efforts that sought to understand the relationship between two arrangement of the bridge pier shape, and scour behaviour, with a specific focus on triangular configurations and the distance between them.

## 1.2 Study Objectives

The research study was conducted in the Hydraulic Laboratory of the Civil Engineering Department at Zakir Hussain College of Engineering & Technology, Aligarh Muslim University, India (Anand & Beg, 2024). Whereas the collected experimental data from one of the models that will later be used for numerical simulations using Flow-3D software to validate model's findings. To carry out experiments on the group of three piers set in a staggered triangular way. the experimental was conducted 6 various models of triangular group of bridge pier and singular bridge pier, the pier diameter were 4 cm in all cases. The singular bridge pier used in the experimental work as reference model. Later in CFD simulation will used as calibration model to validate the model results. Following the calibration of the single-pier model, five triangular pier group configurations were simulated. These cases differ only in the center-to-center spacing between the head pier and the base piers, expressed as the non-dimensional ratio Z/b (Z = distance between head and base piers, b = pier diameter = 4.0 cm). The selected Z/b values (1–25) cover a range of interaction scenarios, from strong interference at close spacing to nearly isolated conditions, as summarized in Table 3.5 and illustrated in Figures 3.7–3.8.

The objectives of this researcher will fucose on studying how the arrangement and shape of bridge piers can affect the development of scour around triangular pier configurations that used in bridge structures, to show how the changing of distance between the piers influences the flow characteristics, the scour depth, and sediment transport. This study aims to achieve several important research and scientific objectives, including:

1. To analyse the behaviour of local scour around a triangular arrangement of circular piers using numerical modelling.
2. To compare the depth and shape of scour in the triangular configuration with traditional cases (single or paired piers), in order to determine the impact of the geometric arrangement on scour severity.
3. To understand the influence of the distance between the bridge pier on the scour behaviour in tow triangular configurations.

4. To validate the results using singular bridge pier by comparing them with data from previous studies and assessing the agreement between numerical models and experimental findings.

### 1.3 Thesis Structure

There are six major chapters in this thesis:

Introduction (Chapter 1): Explaining the context of introduction scope, significance, goals, and thesis structure of the local study in the introduction.
Review of Literature (Chapter 2): Exploring earlier research on local scour at bridge piers, emphasising pier groups, hydrodynamic interactions,
Methodology (Chapter 3): in this chapter the experimental setup and numerical modelling methodology, including pier configurations, flow conditions, measurement methods, and model validation are covered.
Results and Discussion (Chapter 4): Outlines the study's findings, including velocity field analysis, scour evolution, and model comparison.
Conclusions and Recommendations (Chapter 5): Summarizes key findings, highlights contributions, and provides practical recommendations for engineers and suggestions for future research.
References and Appendices (Chapter 6) Lists all the references cited in the thesis and provides supplementary material used in the study.

# CHAPTER 2
# LITERATURE REVIEW

## 2.1 Overview of Local Scour

Local scour occurs when flowing water accelerates and splits around bridge piers, giving rise to a horseshoe vortex at the upstream face and wake vortices downstream that progressively erosive the bed material, Scour holes that are increasing and risking the foundation's stability. Even moderate scour depths can expose pier footings, weakening load–bearing capacity and intensifying the risk of collapse under higher flows.

Early study focused on isolated, single cylinder piers, resulting in well-established empirical correlations based on equilibrium scour depth relationships and Shields parameter scaling. However, applying these findings to grouped pier designs has proven insufficient yet. In multi-pier systems, upstream wake interactions modify the local flow field influence on downstream components, causing interference effects that can either increase or inhibit sediment removal depending on spacing and arrangement (Khaple et al., 2017) (Beg, 2010). The triangular configuration of circular piers creates complex three-dimensional vortical structures and flow interdependence. The triangular configuration of circular piers significantly influences the flow dynamics and scour evolution, necessitating targeted numerical investigations (Abed & Majeed, 2020). Research indicates that the spatial distribution and inter-pier spacing directly affect the scour depth and patterns around these piers. This highlights the need for targeted numerical investigations to understand how spatial distribution and inter-pier spacing affect scour evolution and develop more effective design guidelines. This chapter will cover overview of scour process, scour mechanism, the main factors that influence of local scour phenomena and highlight over the previous studies in the following sections.

## 2.2 Types of Scours

When water flowing over a bridge element interacts with the riverbed in many different kinds of ways, often changing the bed level (Chee, 1982; Ettema, 1980). These changes, also known as scour, can occur for several of causes and are divided into three categories: general scour, localized (or constricted) scour, and local scour. Each kind has unique reasons and consequences for bridge stability (Bettess, 2002).

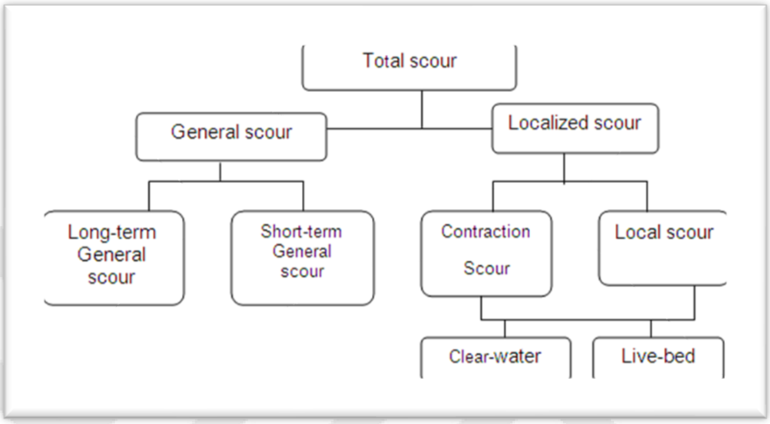


**Figure 2. 1** Scour type illustration chart

1. General Scour

General scour is the broad, natural shifting of the riverbed over time. It happens with or without a bridge in place and is usually driven by big-picture changes in the river's environment (Bettess, 2002).

- The long-term General Scour

This type of scour occurs gradually changing over years or even decades in river bed elevations throughout natural processes like as sediment transportations (aggradations and degradations) or can human interventions such as dam construction, deforestation, and groundwater exploitation. These changes influence on reduce the riverbed over time, putting bridge foundations at danger.

- Short-Term General Scour

In contrast, this type of scour occurs quickly, usually during floods or major storms. The riverbed might temporarily erode due to strong flows but can often recover once water levels return to normal.

2. Localized Scour (Constriction Scour)

occurs when the river's flow is passes through a small opening under a bridge span. With present of piers or abutments that led to narrow the channel, the water speeds up and becomes more turbulent. This additional water flow energy scours the bed and it influencing in move sever way during floods, when massive amounts of water flow through bridge opening.

3. Local Scour

Local scour is quite limited, occurring directly around the base of a bridge pier or abutment. When these constructions obstruct the flow, they generate complicated currents such as vortices (swishing water), which dive into the riverbed and form deep holes around their foundations. This form of scour is one of the most serious challenges in bridge design and safety.

Depending on the movement of sediment in the river, local scour can take two forms:

- Clear-Water Scour

When the water flowing into the area around the bridge pier without being carrying sediment. The flowing water cause scouring in the bed around the bridge pier, but therefore carries nothing to refill the hole, even temporarily. As a result, cleaning clear water can lead to deep, sharp cleaning holes over time.

- Live-Bed Scour

In this case, sediment is constantly moving with the water—into and out of the scour hole. It usually occurs during high flows or floods. Because some of the eroded material is replaced, live-bed scour tends to be less deep than clear-water scour, but it can still be dangerous during peak flows.

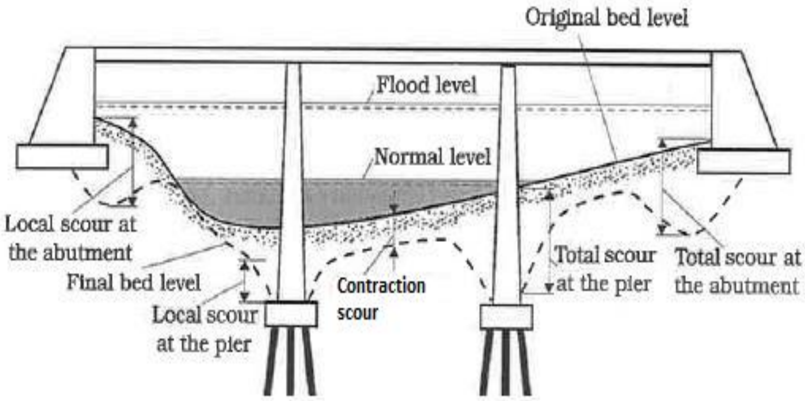


**Figure 2. 2** Illustration the location and form of scour below the bridge components.

### 2.3 Mechanisms of Scour

Scour mechanisms are intricate processes that are impacted by a number of structural and environmental variables. Material around structures like bridge foundations erodes as a result of scour, which is mostly caused by the interaction of flowing water and silt. Predicting the depth of scour and putting effective countermeasures in place depend on an understanding of these mechanisms. Therefore, describe the salient features of scour mechanisms in the sections that follow.

Scouring around bridge piers is a complex process that involves several mechanisms. According to Melville (1975), the primary mechanism is the downflow impinging on the bed at the pier face. When the flow approaches the pier, it slows down and comes to rest, leading to the formation of stagnation pressures that are strongest near the surface and weaken downwards. The flow creates a maximum immediately below the bed level due to the downward pressure gradient at the pier face. This maximum downflow velocity contributes to sediment scouring from the bed and is responsible for the primary scouring mechanism. Another important mechanism is the formation of a lee eddy, also known as the horseshoe vortex, around the pier. The horseshoe vortex effectively transports dislodged particles away from the pier and releases them downstream. It also pushes the maximum downflow velocity within the scour hole closer to the pier, further intensifying the scouring process. Several studies have been carried out on scouring phenomenon around the bridge pier by various researchers such as Chabert & Engeldinger (1956), Kothyari et al. (1992a), Arneson et al. (2012), Sheppard et al. (2014), Kaveh et al. (2021), Wang et al. (2022), and Baranwal et al. (2023a, 2023b). The existence and importance of the horseshoe vortex in the

scouring process around bridge piers have been confirmed by Muzzammil & Gangadhariah (2003), Dey & Raikar (2007), Sheppard et al. (2014) and Zhao (2022). The observation of the horseshoe vortex in the vertical plane is presented in Figure 1(a) and 1(b). Briaud & Oh (2010) reported that all the layer characteristics of the soil could vary significantly with depth and with different erosion functions. Therefore, it is necessary to have an accumulation process that can handle a multi-layer system (Mylonakis et al. 1997; Briaud et al. 2005). Pokharel (2017) evaluated and attempted to understand bridge pier scour depth estimation using a multi-layer method in which the bed sediment (d50) value is calculated layer by layer and compared the final scour depths with the HEC-18 equation in which the d50 value is taken as the average of all layers of the soil. It is reported that using only the average d50 value does not accurately predict the scour depth, and the d50 value of all layers should be considered while calculating the scour depth (Pokharel 2017). A method called the ESRICOS method (Briaud et al. 1999, 2001; Kwak 2001) is proposed to predict the local scour depth versus time curve around bridge piers. This method makes it possible to handle multi-layer soil systems. Jia et al. (2023) conducted a study on inertial and kinematic interactions of bridge-pile groups on liquefiable multi-layer soil-induced lateral spreading and reported that a weak earthquake caused no significant seismic response under the bridge. The saturated sand displayed dilatant behavior, enhancing the acceleration peak response during the intense earthquake. Tison (1940) laid the foundation for further research in the field of bridge pier scour and helped to better understand the factors that contribute to equilibrium scour depth around different shapes of bridge piers. Since then, numerous studies have been conducted to improve our understanding of bridge pier scour and to develop effective methods to mitigate its impacts

### 2.3.1 Scour Process and Scour Hole Formation

Vijayasree et al. (2019).Choi and Choi (2016); Melville and Raudkivi (1977); Niedoroda and Dalton (1982); Tan et al. (2020) They describe the process of scour, when a bridge pier blocks a waterway, water accumulates up on the pier's front face and the flow accelerates up around the pier face, converting unidirectional water flow into three-dimensional flow. This occurrence causes a horseshoe-shaped vortex to form at the bottom of the bridge pier, while a wake vortex is an upward-moving vortex that forms downstream of the pier, Besides when the increasing of water level in front of piers or abutments after the water hit it, resulting from of reduction in speed of water flow that leads caused stagnation pressure of the water created a downward flow result in horseshoe vortex, the vertical component of the downward flow causes erosion around the bed material around the pier as shown in Figure 2.4.

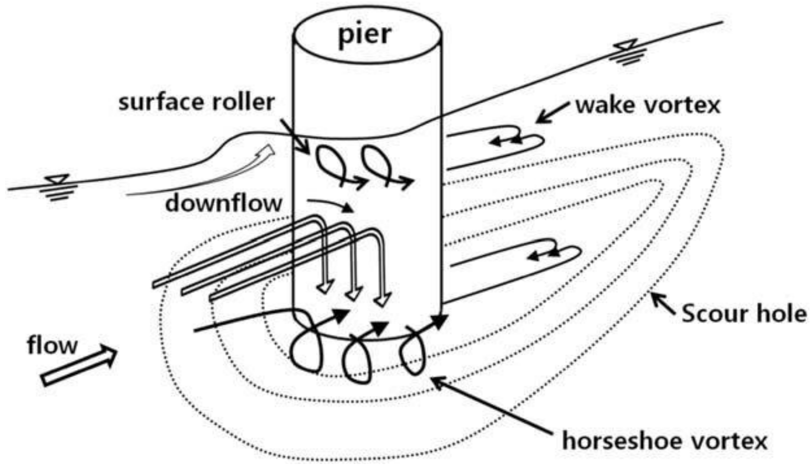


**Figure 2. 3** mechanism of Local scour around a bridge pier Choi and Choi (2016)

These vortices remove sediment, creating a scour hole downstream, this process weakens the foundation by reducing the support of the pier's foundations. As shown in figure 2.3. The "scour hole," also known as the scour depth, is a crucial metric for assessing about severity of the erosions (Brethour, 2003; Dargahi, 1990; Lu et al., 2008; Melville & Raudkivi, 1977; Muzzammil et al., 2000; Wang, Yu, et al., 2017).

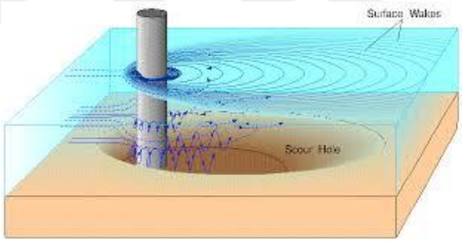


**Figure 2. 4** Scour hole around a bridge pier (Vijayasree et al., 2019)

Figure 2.4 illustrates how the flow direction splits into three distinct movements when the flow field encounters obstruction: wake vortices, the horseshoe vortex, and down-flow. These motions are described in the sections that follow.

### 2.3.2 Downflow in the front of the piers

A stagnation point will form at the bridge pier's front surface whenever the flow field hits the pier's frontage, increasing the water flow depth. This results in the beginning of a pressure difference between the upstream and stagnant sides. The depth of flow is also influenced by the fluid's shape and speed. The pressure also decreases when the flow velocity in front of the pier decreases since it is reliant on the approach velocity.

### 2.3.3 Horseshoe vortex

The term "horseshoe vortex" is used in the literature to describe vertical vortices that flow around a pier because of the form of the vortex. The system horseshoe vortex naturally occurs when a scours hole is formed. When the downstream and incoming flows are coupled, a horseshoe-shaped vortex system will occur. For this, the vortex flow travels downstream along the pier edges, as seen in Figure 2.4. The strength of the horseshoe vortex is determined by the turbulent flow and the shape or geometry of the pier (Unger & Hager, 2005).

### 2.3.4 Wake Vortices

The wake vortexes formed when a flow divides as it passes over the edges of a pier are seen in Figure 2.4. These wake vortexes also contribute to the material deterioration around the bridge pier. Melville and Raudkivi (1977) detailed that wake vortexes travel downstream, causing downstream and horseshoe-shaped vortices to carry sediments.

## 2.4 Factors affecting Scour Mechanisms

### 2.4.1 Flow Characteristics:

The flow velocity and direction significantly impact scour initiation. Higher velocities increase bed shear stress, leading to greater sediment transport and erosion.

### 2.4.2 Sediment classification and its Physical characteristics:

The size and gradation of sediment particles, sediment type and roughness are important role in the scour development process. As example finer sediments are more easily eroded, whereas coarser materials provide greater resistance (Kleinhans et al., 2017). Cohesive soils show different erosion behaviors than granular materials (Palermo et al., 2024). Also, Temporal variations in scour depth are also influenced by sediment characteristics, with different materials responding uniquely to hydraulic forces (Kleinhans et al., 2017).

### 2.4.3 Effect Of Bridge Pier Shape on Scour Depth and Scour Development

The design of the shape of a bridge pier is a crucial factor in determining the amount of local scour it will undergo. Chabert & Engeldinger (1956) classified the pier shape into blunt-nosed and sharp-nosed. The formation of a horseshoe vortex system around the upstream nose of the pier, where most scour occurs, defines a blunt-nosed pier. On the other hand, a sharp-nosed pier splits the flow and experiments have shown that a horseshoe vortex system does not form around its upstream face. As a result, no scour occurs at the sharp-nosed shape of the bridge pier when it is properly aligned with the flow. However, if tested at an angle to the flow, the bridge pier transforms into a blunt-nosed pier, leading to deeper scour. Many researchers have studied different bridge pier shapes such as chamfered, cylindrical, diamond, elliptic, flared, hexagonal, joukowsky, lenticular, oblong, octagonal, sharp nose, square, rectangular, round-nosed, and triangular (Tison 1940;Inglis 1949; Chabert & Engeldinger 1956; Shen et al. 1966; Ettema 1980; Chiew & Melville 1987; Kumar et al. 1999;Ettema et al. 2006; Hassanzadeh et al. 2019; Garg et al. 2022; Baranwal et al. 2023a).

The geometry of bridge piers, as Figure 2.5 shows a schematic illustration of some pier shapes, affects flow patterns and vortex formation, which can enhance local scour around foundations. Vortex formation and sediment entrainment are determined by the pier cross-section, which also controls how incoming flow navigates the barrier (Jahangirzadeh et al., 2014). Cylindrical piers esteemed for their structural simplicity, foster strong, symmetric horseshoe vortices and coherent wake shedding, concentrating erosive power at the base and producing deep, rounded scour holes (Jalal & Hassan, 2020). In contrast, streamlined or oblong profiles promote smoother flow attachment, elongate the separation zone, and weaken downstream vortices, yielding shallower, more elongated scour depressions. Sharp-nosed piers further deflect the incoming current, reducing adverse pressure gradients at the bed and curbing sediment uplift (Abed & Majeed, 2020).

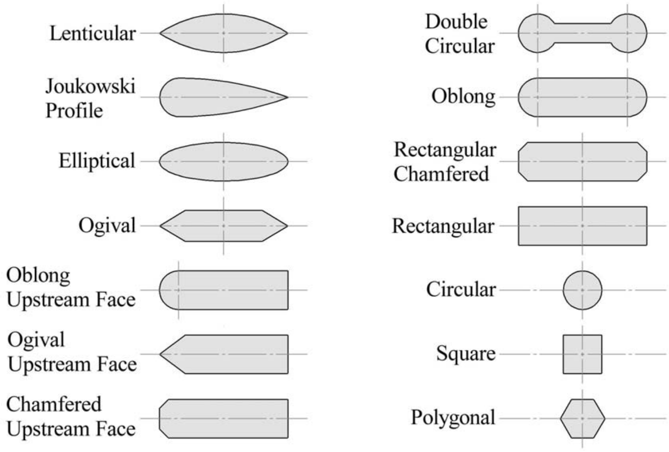


**Figure 2. 5** illustration of some pier shapes.

### 2.4.4 Shields Parameter, Critical Shear Stress

Sediment entrainment depends on the interaction between fluid-induced shear stresses and gravity forces that control particle movement (Zordan et al., 2018). The dimensionless Shields parameter θ encapsulates this balance, comparing bed shear stress to the threshold needed to mobilize grains. When θ exceeds its critical value θ_c, local bed material starts into motion, initiating scour(Zordan et al., 2018). This removal continues until the bed geometry—and thus the local shear stress—adjusts to a configuration where θ Retreats back to θ_c, until reaches of equilibrium scour depth.

### 2.4.5 Time Evolution of Scour Holes (equilibrium scour depth)

The idea of equilibrium scour conditions is widely mentioned in the literature. According to (Hoffmans, 1998), equilibrium is the condition of scouring in which no additional change occurs over time. The progression of a scour hole occurs in two distinct phases: an initial rapid deepening characterized by vigorous vortical activity, followed by a slowdown as the hole enlarges and vortex strength diminishes. During the initial phase, high-energy vortices and loose sediment interact to excavate material quickly, while the subsequent phase sees a transition to a more stable scour profile (Zordan et al., 2018).

Both live-bed and clear-water sediment transport conditions can cause local scour. In live-bed settings, equilibrium scour depth is attained when the average quantity of sediment entering the scour hole and the amount exiting it is equal, this condition is reached much faster than in clear-water flow conditions and varies around an average value. as seen in Figure 2.6.

In clear-water conditions, equilibrium scour depth is achieved when the flow can no longer remove sediment particles from the scour hole. (Akhlaghi et al., 2020; Chabert, 1956).) concluded that equilibrium occurs when the scour depth does not change "significantly" over time. Ettema (1980) standard three well-defined phases of the scour mechanism, which are defined as follows:

1. **Initial Phase**: Characterized by rapid scouring due to downflow at the upstream face of the pier. During this phase, the horseshoe vortex is not significant, and sediment transport begins on the sides of the pier.

2. **Principal Phase**: Controlled by the activity of the horseshoe vortex, this phase sees scour occurring in a narrow section around the pier. As the scour hole develops, the strength of the horseshoe vortex and the downflow gradually become insufficient to transport sediment from the bed erosion zone.

3. **Equilibrium Phase**: Reached when there is no further significant development in the scour hole.

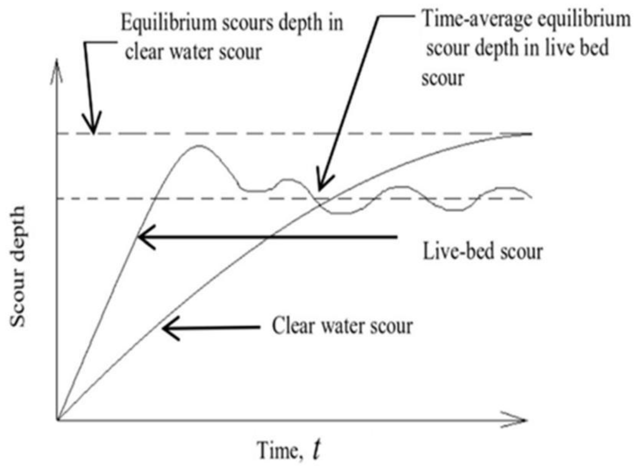


**Figure 2. 6** Scour depth development vs. time in clearwater and live-bed conditions (Akhlaghi et al., 2020; Chabert, 1956).

### 2.4.6 Classification of Pier Groups (In line, Side-by-Side, Triangular)

Group of piers, whether in line or side-by-side or triangular arrangements, making the stream flow around the Group of bridge piers more complex and increasing its turbulence. Their spatial arrangement influences the forms of scour holes. In an in-line or tandem plan (Aligned parallel to the direction of the current), piers sequentially aligned with the main flow axis yield a downstream structure protected by the following of its predecessor, producing stream flow for each downstream pier lies both in the wake of an upstream neighbor and in a side flow from another, creating intersecting vortical systems and accelerated corridors of high shear velocity.

- Longitudinal Arrangement (Row or Tandem)

In this case, the first front pier that is facing the flow is more affected because it receives the accelerating flow, the second rear pier is situated in the shadow of the first pier, meaning that scour around it may be lighter due to the influence of the first pier.

This provides a form of protection for the rear pier from strong currents and erosion forces.

- Side-by-side Arrangement

The piers are side-by-side (parallel to the direction of the current), so that the current flow field splits between the piers, producing horseshoe vortices on each pier’s side. it may merge and cause a deeper scour hole in the area between the piers.

- Triangular or Staggered Arrangement

Each rear pier is partially in the shadow of the pier in front of it and partially in a side current coming from the front pier. Each rear pier is partially in the shadow of the pier ahead of it and partially affected by a side stream flowing from the front pier. This creates a complex vortex system and the flow passages with higher shear velocity. This arrangement is used on wide rivers, not only for structural stability, but also because of its distinctive effect on water movement.

### 2.4.7 Interaction Effects the Mechanism of Local Scour in Grouped Pier Formations

When a group of bridge piers are installed close to one another they disrupt water movement in ways that are more complex than from a single pier. So, each one creates a wake vortex that a disturbed zone behind it which can interfere with how the current reaches nearby piers. interactions from this process resulting in unpredictable patterns that affect scouring around the foundations (Malik & Setia, 2021; Sang et al., 2022).

In other arrangements, such as when the piers are placed in a triangle, the water flows that form behind each pier cross over each other at an angle (Akhlaghi et al., 2020). This creates small zones where the water either speeds up or slows down sharply (Malik & Setia, 2020). Thus, these conditions are quite different from what happens when only one pier is present in the water. In other arrangements like when piers are arranged in a triangular configuration, the water flowing behind each pier tends to cross paths at different angles(Akhlaghi et al., 2020). These intersecting flows can create small areas where the speed of the water suddenly increases or drops off (Malik & Setia, 2020). This kind of flow behavior is noticeably different from what usually happens around a single pier placed on its own (Akhlaghi et al., 2020; Malik & Setia, 2020).

### 2.4.8 Experimental Studies on Two- and Three-Pier Groups

In research was conducted by Malik and Setia (2020). A group of experiments were carried out in the Hydraulics Laboratory of National Institute of Technology Kurukshetra India. An experimental study was conducted on a bed with a recirculating flume 15 m long, 0.40 m wide and 0.60 m high was used. The working section provided at 5 m downstream from the inlet section in the flume. The working section assuming it to be a section where the flow was fully established. A tailgate has been provided at the end of the flume to control the depth flow and velocity of flow. Two different size circular piers 62 mm and 42 mm external diameter were used for the experimental study. Experiments were carried out with three different sizes of sediments 0.23 mm, 0.30 mm and 0.50 mm. Figure 2.6 shows a systematic line diagram of two circular piers in a line. The study used cylindrical pier models with a diameter of 4.2 Cm. These models were tested in three different arrangements: Tandem, Side by Side, and Staggered Figure 2.7 and 2.8. Each arrangement was designed to analyze how the spacing and orientation of the piers affected the scour depth**.** The experiments were conducted at a flow velocity of 0.89 times the critical velocity.

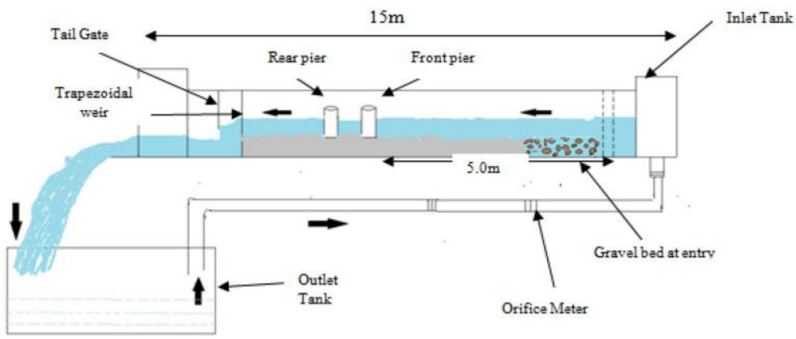


**Figure 2. 7** A methodical drawing of recirculating flume utilized in the experimental study

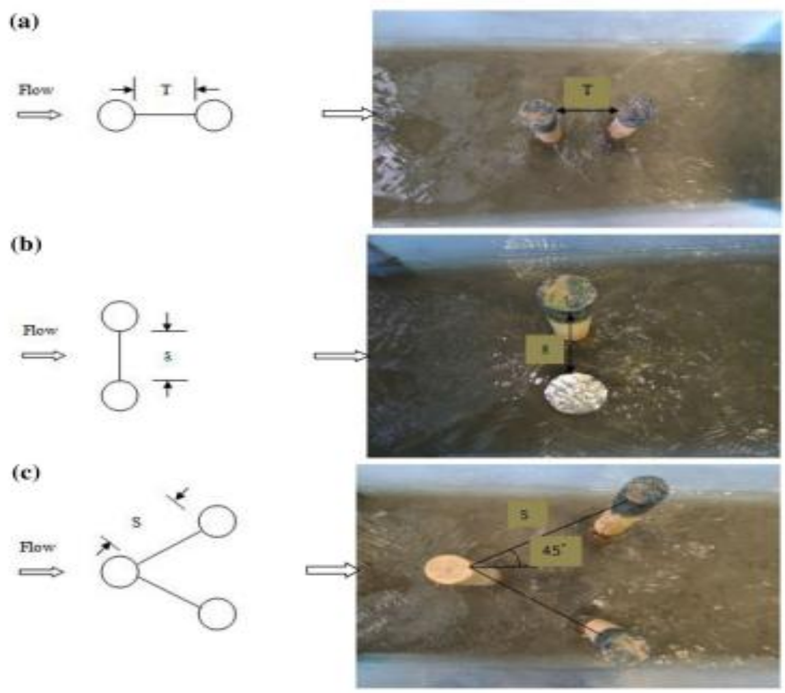


**Figure 2. 8** illustrates schematic representations of various pier arrangements in a flow channel: (a) tandem configuration, T; (b) side-by-side configuration, and (c) staggered configuration involving three piers.

Malik and Setia (2020) showed the positioning of bridge piers plays a essential role. Their study revealed that both arrangement and spacing significantly impact scour hole development. These scour holes are essential for maintaining bridge structural integrity. The research explored several configurations of tandem, side-by-side, and staggered arrangements. Each setup has distinct shapes, flow dynamics, and influences scour depth. The following sections detail these findings. Also, in tandem arrangement: when piers are spaced 16-d times their diameter, they behave independently. however, at closer spacing 0-d, scour depth increases by 41% compared to a single pier, for Side-by-Side and Staggered Arrangements: Independent behavior is observed when spacing exceeds 1.5 times the diameter for side-by-side and 2.5 times for staggered arrangements. The following results are drawn about a tandem arrangement when two piers present in a line: The scour depth around the upstream pier always greater than the downstream pier; When the clear spacing between the piers was T/D = 0the piers behaves as a single pier. But when the clear spacing between the piers increase, the upstream shows a rapid increase in scour depth. The scour depth around the piers depends upon the size of the sediment if the mean size of the sediment large the scour depth found to be the minimum

In estimating the scour depth around the piers, M5models show higher predictive accuracy than ANN models. In addition to this, the comparative study of input data-set concludes better performance by the output data-set. Modelling and experimental results suggest that the influence of sediment size, velocity of flow and diameter is considerably higher than other parameters in affecting the scour depth around the bridge piers. The modelling in the present experimental study is useful in arriving at a combination of flow conditions corresponding to scour depth within the experimental range of this study.

Another investigation carried out by (Malik & Setia, 2021) conducting experiments in a controlled environment using a recirculating flume that was 12 meters long, 0.6 meters wide, and 0.7 meters high. The study utilized circular and oblong pier models with a diameter of 6.2 cm as shown in figure 000. These models were arranged in different configurations: tandem, side by side, and staggered. The sediment used in the experiments had an average size of 0.23 mm. The ratio u/uc comes out to be 0.93. with water depth of flow (cm) 16 to 18.5.

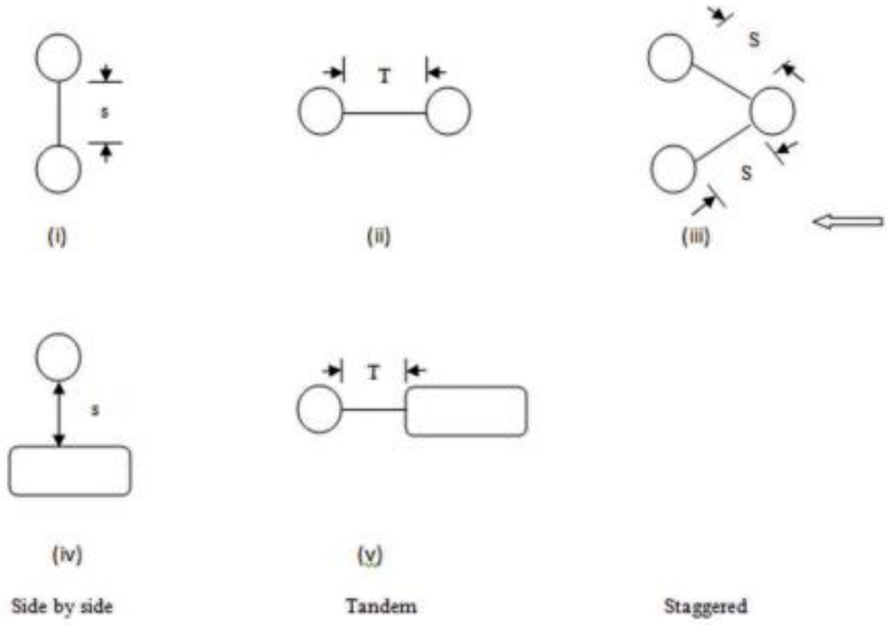


**Figure 2. 9** Definition sketch of different arrangements

The experiments highlighted that the shape and arrangement of bridge piers play a crucial role in determining the scour depth. Understanding these interactions is essential for designing safer bridge foundations, especially in areas where multiple bridges are in close proximity.

### 2.4.9 Importance of Numerical Modeling in Scour Research

Applying laboratory flume experiments yield valuable insights into individual processes, they often hit a wall—limitations in scale, repeatability, and the ability to capture nuanced flow features. Enter Computational Fluid Dynamics (CFD), a dynamic partner for researchers tackling these challenges. CFD empowers researchers to simulate the intricate modeling like of pier, flow, and sediment interactions with comprehensive scour detailed investigations. By dissecting three-dimensional velocity gradients, pressure zones, and turbulence structures, CFD models show the mechanisms of vortices, which can caused transport of sediment with it can avoid some inaccurate records through lab tests. Whoever, researchers can now perform parametric sweeps across varied flow conditions, pier shapes, and sediment properties. This efficiency not only cuts costs but also accelerates the process, marking CFD as an indispensable player in comprehensive scour investigations.

Among available CFD platforms, FLOW-3D stands out for its robust handling of free-surface flows by the Volume of Fluid (VOF) technique and its native sediment-transport modules. Resolving the complete Navier–Stokes equations in tandem with k–ε or RNG turbulence equations it captures both large-scale vortexes and the small one, in control for particle entrainment. Bed deformation changes along the canal by dynamic simulation for local shear stress exceeds critical thresholds, sediment reorganized, carried, and redeposited according to specified grain size distributions. The software's flexible meshing and boundary-condition schemes accommodate realistic channel geometries and support iterative refinement around regions of intense scour activity.

**Study objective**

Triangular arrangements of circular piers are used in real-world bridge foundations to distribute loads and enhance structural performance. Nevertheless, the complex of flow interfering, turbulence, and potential for localized scour intensification within these groups is in position serious challenges to bridge safety. Investigating specific in triangular arrangements configuration provide a more assessment of scour risk and hydraulic behavior comparing with singular piers. Understanding how varying the spacing between the piers in a triangular arrangement's setup influencing the formation and depth of scour holes that can lead to more safety to bridge design.

**2.4.10** Fundamentals of the Initial motion of sediment particles

The primary movements of sediment starts when water flow intensity is enough to pull particles of the bed sediment. The flowing hydrodynamic forces influential on the sediment particles are in charge of their movement (Kanellopoulos 1998). Since sediment is moved throughout the length of a riverbed in a complicated manner, explaining the flow conditions under which sediment will transport might be complex, for this purpose, researches focus on the flow conditions adjacent to sediment's particles initial movement. As shown in Figure 2.8, the forces acting on a sediment particle are mainly composed of four forces: FL denotes the lift force (buoyance), FW represents the force downward from the submerged weight, FR is the resistance force FD is the drag force

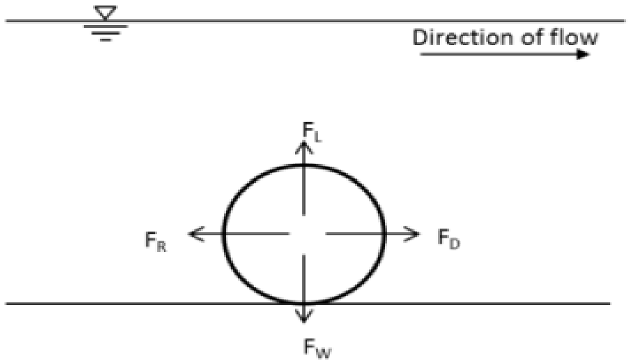


**Figure 2. 10** The main forces influential on a sediment particle and their direction.

Following requirements must be provided in order for beginning motion to start happening:

$$FD = FR \tag{2.1}$$

$$FL = FW \tag{2.2}$$

Numerous factors influence the forces that affect a sediment grain, including lifting power, drag, resistance, and gravity. Shields was the first to show how to advance a relationship between hydraulic factors and sediment characteristics in order to meet the requirements for beginning motion in 1936. Shields investigated situations where bed particles are stable but on the verge of moving by employing dimensional analysis.

Shields discovered that the critical Shields value ($\tau c*$) and the shear Reynolds number (Re*) can be used to determine the critical conditions in which sediment is about to get entrained. The following relationship yields the crucial Shields value, known as the dimensionless shear stress:

$$\tau_{c^*} = \frac{\tau_{bc}}{(\rho s - \rho)ga} \qquad (2.3)$$

where (g) represents gravity and (a) indicates the diameter of the soil particles, $\tau bc$ = ($\rho U*c$) represents critical bed shear stress for the start of motion of the particles, ($U*c$) is the critical shear velocity of flow, and ($\rho s$) indicates the density of the soil particle and $\rho$ is water density.

Reynolds number, or Re is a value without dimensions that indicates the proportion of inertial forces to viscous forces. The primary purpose of the Reynolds number is to indicate whether a flow is laminar or turbulent. Laminar flows occur at low Reynolds numbers where viscous forces predominate, while turbulent flows occur upon high Reynolds numbers when inertial forces predominate. It is also possible to modify the Reynolds number in order to examine the initial motion of sediment particles. The following is the specification for calculating the Reynolds number:

$$Re = \left(\frac{U\, d_{50}}{\nu}\right) \qquad (2.4)$$

ν represents the fluid's kinetic viscosity, U point to the flow velocity, and d50 indicates the median particle diameter of the sediments. Since it utilizes the shear velocity, the shear Reynolds number R* is used when examining starting motion and is calculated as follows:

$$Re *= \left(\frac{U*\ D_{50}}{\nu}\right) \qquad (2.5)$$

where U* corresponds to the flow's shear velocity. The Shields diagram represents a graphical representation of the relation between the dimensionless shear stress ($\tau*c$) and the shear Reynolds number (Re*), describing the values at which the beginning of sediment movement occurs. Since the connection is dimensionless, it is possible to compare the driving forces of particle motion, the density, size of particles and the resistance forces.

The beginning of sediment movement depending not only on hydraulic conditions but also on the physical characteristics of the bed material. The behavior of non-uniform sediment particles is generally more complex than that of uniform sediment particles, as factors such as grain shape, inter-particle interactions, and position on the channel bed they are all influencing on sediment transportation. the Froude number is an important parameter which represents the ratio of inertial to gravitational forces acting on the fluid. It is frequently employed to evaluate the resistance that a surface or object places on the flow of water. A higher Froude number indicates greater resistance from the bed material to the flow. The Froude number is defined as:

$$F_r = \frac{U}{\sqrt{gh}} \qquad (2.6)$$

Here, h represents the flow depth. To evaluate how the Froude number relates to the transport of bed material, a dimensionless form known as the densiometric Froude number is often used. This version expresses the ratio between the inertial forces acting on a sand particle and its submerged weight. The densiometric Froude number is defined as:

$$F_0 = \frac{U}{\sqrt{\frac{g\, d50\ (\rho s-\rho)}{\rho}}} \qquad (2.7)$$

Here, "$d_{50}$" stands for the bed sediment's median particle size. The early motion of uniform sediment has been the subject of numerous studies (Buffington and Montgomery, 1997; Andrey and Gareth, 2000; Vollmer and Kleinhans, 2007; Beheshti and Ataie, 2008), however there is still little information available on the initial motion of non-uniform bed materials. For instance, Xu and Yu (2008) used field data to test their model for incipient velocity, which was based on the balance of uplift and drag forces. According to their research, coarse, non-uniform particles needed a lower critical (incipient) velocity to start moving than uniform sediments. On the other hand, they found that non-uniform sediments needed a higher incipient velocity than their uniform counterparts for finer particles.

## 2.5 Scour Prediction Governing Equations

Many empirical equations were created to determine the local scour depth at the bridge pier according to (McIntosh, J. L.,1989). Local scour equations are classified based on the type of local scour if it's clear water scour or live-bed scours, local scour equations can be developed using different methods like curveting and regression method to compute maximum scour depths. There are some equations to compute the scour depth:

### 2.5.1 Breusers Equation

The local scour depth equation developed by (Breusers 1965) concluded, that the maximum scours depth was affected by pier diameter where the maximum scour depth was about 1.4 times the pier diameter.

$$d_s = 1.4b \qquad (2.8)$$

where $b$ is pier diameter and $d_s$ maximum scour depth.

### 2.5.2 Laursen Equation

Laursen and Toch (1956) depend on an experimental study for the development of scouring equations through the reflection of the flow depth in computing scour depth. While Shen (1966) depend on the velocity for the development scour equation by with Froude number. The next formula (Laursen and Toch) is for square-nosed piers Les Hamill, (1999) Bridge hydraulic.

For Live bed scour: $$d_{sp} = 1.5\ b_p\ 0.7Y0.3 \qquad (2.9)$$

For Clear water scour: $$d_{sp} = 1.35\ b_p\ 0.7Y0.3 \qquad (2.10)$$

Where, $d_{sp}$ is the pier scour depth (m), $b_p$ is width of the pier (m), y is the depth of approach flow (m). Also, Shen II equation is written

$$d_{sp} = 3.4\ bp\ 0.67\ F\ 0.67\ Y0.33 \qquad (2.11)$$

Where the Froude number F of the approach flow.

### 2.5.3 Larras equation

Larras (1963) depends on field data from several French rivers to develop Larras equation:

$$y_s = 1.42\ K_{S2}\ b0.75 \qquad (2.12)$$

where the coefficient $K_{S2}$ is based on the shape of the pier nose (1.0 for cylindrical piers and 1.4 for rectangular piers) Where $y_s$ and b in ft. Larras measured scour depth after a flood had passed, this equation depends on pier width and shape only (Shen and others, 1969).

### 2.5.4 (HEC-18) Pier Scour Equation

The HEC-18 pier scours equation can calculate both live-bed and clear-water pier scour, Maximum pier scours depths are predicted by the equation, Simple pier structure configurations and riverine flow conditions in bed channels are examples of basic applications. The HEC-18 equation has developed over time and is now one of the FHWA's recommended methods for estimating evaluating equilibrium scour depths at simple piers (Arneson et al.2012).

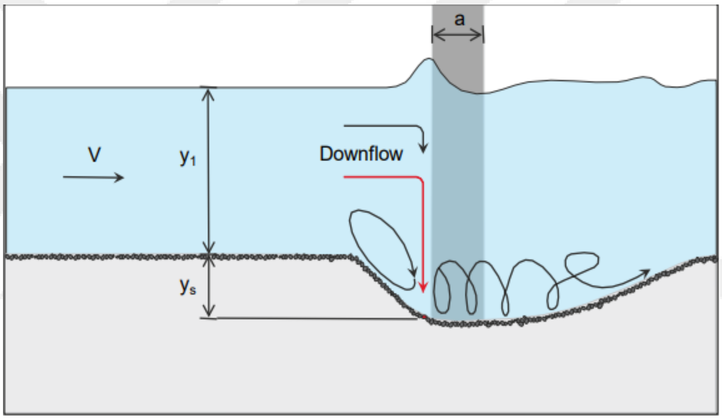


**Figure 2. 11** Description sketch for pier scour (Arneson et al.2012).

(Arneson et al.2012) presents (HEC-18) equations for circular piers scour as:

$$\frac{ys}{y1} = 2\ K_1 K_2 K_3 \left(\frac{a}{y1}\right)^{0.65} F_{r1}^{\ 0.43} \qquad (2.13)$$

from Figure 2.10 and Figure 2.11 can described parameters of (HEC-18) equation as following:

ys = Scour depth. y1 = Flow depth directly upstream of the pier.

K1 = Correction factor of pier nose shape.

K2 = Correction factor of the angle of flow attack.

K3 = Correction factor of bed condition.

a = Pier width. L = Length of the pier.

$F_{r1}$ = Froude Number directly upstream of the pier.

Where a coefficient $K_1$ based on the shape of pier nose from Figure 2.10 ($K_1$ = 1.1 square-nosed piers, 1 for circular nosed pliers, and 0.9 for sharp-nosed pier), the coefficient $K_2$ based on the ratio of the pier length to the pier width (L/a) and alignment of the approach flow to a bridge pier, (Table 2.2) also, Table 2.3 below show the Coefficient for pier alignment and Bed-condition correction factor ($K_3$) (Arneson et al.2012).

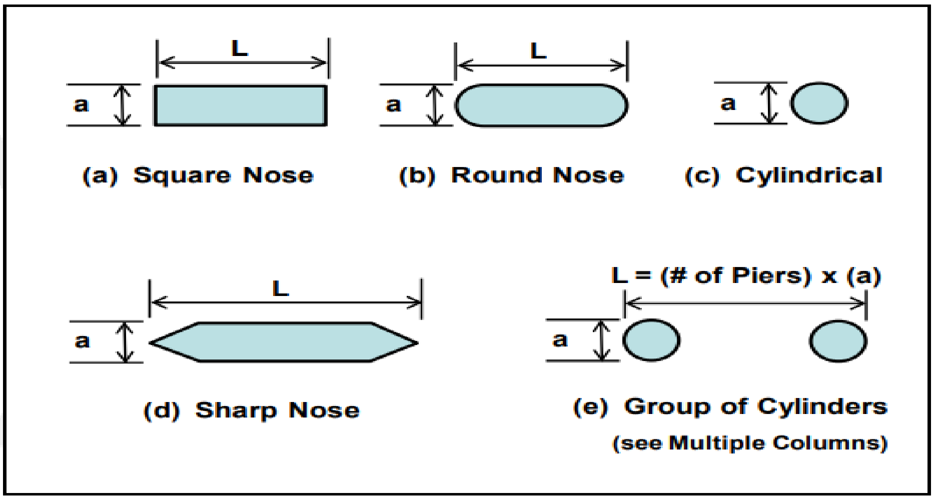


**Figure 2. 12** Common Pier Shapes (Arneson et al.2012).

**Table 2. 1** Coefficient for pier alignment (K2)

| Angle | L/B=4 | L/B=8 | L/B=12 |
|---|---|---|---|
| 0° | 1 | 1 | 1 |
| 15° | 1.5 | 2 | 2.5 |
| 30° | 2 | 2.75 | 3.5 |
| 45° | 2.3 | 3.3 | 4.3 |
| 90° | 2.5 | 3.9 | 5 |

**Table 2. 2** Correction factor for the increase in equilibrium scour depths (K3).

| Bed Condition | Dune height m | K3 |
|---|---|---|
| Clear-water scour | N/A | 1.1 |
| Plane bed and anti-dune flow | N/A | 1.1 |

| | | |
|---|---|---|
| Small dunes | 0.6 to 3.0 | 1.1 |
| Medium dunes | 3.0 to 9.0 | 1.1 to 1.2 |
| Large dunes | > 9.1 | 1.3 |

**2.6 CFD Numerical Simulation**

Before the advent of the technology of the computer, experimental models were frequently utilized for building great hydraulic structures. For example, designing dam and canal. Physical modelling in turbulent flow has challenging underpinnings based on observations of traffic-induced vibrations, first method relies on modal identification for bridge spans, while the other relies on monitoring the dynamic reaction of the pier foundations (Mehaladevi, P., and Venkatesh, A. 2020). With the growth of technology and software in the world, computational models are becoming more reliable and are regarded as a perfect economic tool for engineering design. A computational fluid dynamic model CFD for hydraulic engineering is an upgraded version of CFD that was first created for mechanical engineering. Computational modelling investigations are now important for designing hydraulic engineering projects, like watershed estimates, and river studies.

To study local scour development as a result of turbulence, simulations with a more detailed turbulent flow field are necessary. Turbulent model equations begin with the standard K-ε model, where explains two transport equations for turbulent kinetic energy as well as its dispersion rate for eddy viscosity estimations. In addition to the standard K-ε model, many modified K-ε models, for case, renormalized and realizable K-ε models similarly exist for complicated flow fields around bridge piers. as yet, the applicability of each turbulence closure model to the turbulent flow field close bridge piers remains unknown. As a result, it emphasizes the importance of developing an appropriate turbulence model for simulating the turbulence flow field around bridge piers.

Olsen and Melaaen (1993) offered out research under steady flow to examine local scour nearby pier using the numerical modelling by means three-dimensional flow and finite-volume method, The $K - \varepsilon$ turbulence modelling was applied to solve non-transient (Navier-Stokes) equations and the Reynolds-stress respectively. Investigated the mechanism of flow especially the laminar horseshoe vortex flow at the crossing between a level plate and a circular pier (Briley and McDonald1981). The large-ability and high quality of computers since the 1990s quickly improved the field of numerical modelling. (Deng and Piquet1992) examined the horseshoe vortex using the algebraic Baldwin-Lomax turbulence modelling.

Roulund et al. (2005), 3D Model investigated numerically and experimentally the flow nearby circular piers which offered by to steady flow. The horseshoe vortex impact, the lee-wake vortex was studied, also the Reynolds number and the bed roughness was reviewed. In the latter study, the steady resolution solve of the model was selected.

By Eulerian approach (VOF) system, local scour with Free Water Surface (FWS) has been numerically investigated and the finding is compared with observed results. Promising results accomplished from the model.

Ahmad et al. (2015) applied the 3D computational fluid dynamic REEF3D modelled under wave conditions to study to physics of local scour then compared with experimental results as shown in Figure 2.11 good agreement obtained

1. Scour under wave act increases utilizing time till steady state is reached.

2. Bridge piers with the side-by-side arrangement of the lead to a contraction development and causes more scouring between the bridge opening.

3. Piers with a triangular arrangement and equal spacing among the piers decrease scour rate.

4. The triangular arrangement leads to a decrease in scour depth as compared to the side-by-side arrangement of the piers.

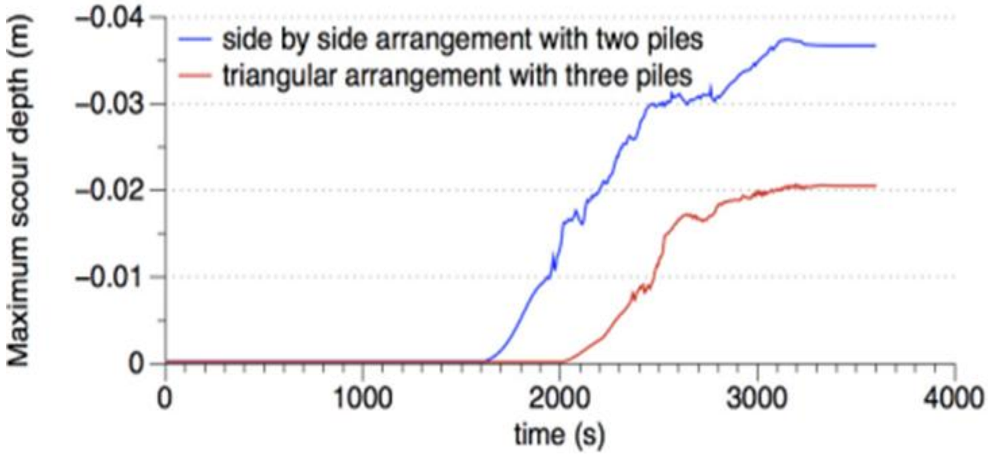


**Figure 2. 13** Time-based variations of the local scour around the side-by-side arrangement compared to the triangular arrangement of the piers(Ahmad et al., 2015) .

In this work, FLOW-3D has been used to simulation the purposes. It allows various non-cohesive types and analyzes deposition, entrainment, bedload transfer, and suspended load transport when fully coupled with fluid flow. Volume and area fraction that describes the packed sediment are calculated throughout the whole domain at every time step that is being incorporated by the user. Bed shear stress, the critical shield parameter, erosion rate, bedload transport rate etc. are calculated at each mesh cells of the sediment bed for better prediction in the sediment scouring process. Bed shear stress is calculated employing a standard wall meaning that estimates the bed surface roughness which is relevant to the medium grain size $d_{50}$. The sediment scours model undertakes different sediment types with diverse properties counting grain size, critical shear stress, mass density, angle of repose and parameters for entrainment and conveyance. The model is applied to measure bedload transport, suspended load transport, sediment transport process, entrainment also deposition of sediment. Where entrainment is the process that moves the sediment from the packed bed facade and moved to a different site. This phenomenon can be only observed when the bed shear stress exceeds the critical value of the shear stress. On the other hand, deposition is the process wherever sediment from the outward area come into the packed bed field due to the effects of different factors such as friction, gravity and buoyancy effect. The bed load means; the particles in the flowing fluid that are transported onward with the bed. Bedload movement means the movement of bed load by rolling, sliding and saltating.

## 2.7 CFD Equations for Bedload Transport

### 2.7.1 Bed shear stress:

It is shearing stress that is stuck on the bed and measured by wall function for 3D turbulence flows.

$$u = u_\tau \left[ \frac{1}{k} In \left( \frac{Y}{\frac{v}{u_\tau} + k_s} \right) \right] \tag{2.14}$$

Where: $u\tau$ = the shear velocity, $u\tau = \sqrt{\frac{\tau}{\rho}}$ , τ = bed shear stress and ρ=bulk density of the fluid-sediment mixture, Y= distance from the wall, ν = kinematic viscosity of the bulk flow, K= 0.4 is the Von Karman Constant and $ks$ is related to the grain size and can be defined as:

$$ks = Csd50 \tag{2.15}$$

$d50$ = Median grain diameter of the bed material, $Cs$ = user-defined coefficient, usually recommended value is 2.5.

### 2.7.2 Critical shields parameter

It's a type of bed shear stress that has no dimensions. The default value of $\Theta cr,n$ is a horizontal and level bed of similarly sized grains. It can be measured by users (by default, 0.05) or calculated using the Soulsby-Whitehouse equation (Soulsby and Whitehouse, 1997),

$$\theta_{cr,n} = \frac{0.3}{1+1.2d_{*,n}} + 0.055(1 - e^{-0.02d_{*,n}}) \tag{2.16}$$

And here $d_{*,n}$ is dimensionless grain size, written as

$$d_{*,n} = dn[\frac{g(S_n-1)}{v_f^2}] \tag{2.17}$$

Here, $S_{,n} = [\frac{P_n}{P_f}]$, and $v_f$= kinematic viscosity of the fluid.

### 2.7.3 Entrainment and deposition

These two are considered as exactly opposite micro-processes that occur during a similar time. The combined effect of these two is calculated for the net rate of exchange among suspended and packed sediment. During entrainment, the velocity at which the sediment leaves the packed bed is called lifting velocity. And this velocity can be calculated by (Winterwerp et al. 1992), the entrainment coefficient of species $n$ (default value is 0.018), and $n_b$ is the outward typical vector of the packed bed surface. In a deposition, the settling velocity of Soulsby (1997) is used,

$$u_{lift,n} = n_b \alpha_n {d_{*,n}}^{0.3} \left(\theta_n - \boldsymbol{\theta_{cr,n}}\right)^{1.5} \sqrt{g d_n (s_n - 1)} \qquad (2.18)$$

$$u_{lift,n=} \, n_b \, n$$

### 2.7.4 Bedload transport

bedload transport parameter that has no dimensions can be defined by the equation where, $q_{b,n}$ is the volumetric bed load transportation rate per unit of bed width (in units of volume per width per time). $\Phi_n$ is determinate using the Meyer-Peter and Muller equation (1948),

$$\Phi_n = B_n \left(\Theta_n - \Theta_{cr,n}\right)^{1.5} C_{b,n} \qquad (2.19)$$

Where $B_n$ is the bed load coefficient. generally, 5.0 to 5.7 for lowest transport, around 8.0 for intermediary transport, and up to 13.0 for very large transport. For the FLOW3D the value assigned for bedload transport is 8.0 and which is the most common value found from the analysis of literature. $And\ C_{b,n}$ is the volume fraction of species $n$ in the bed material which can be expressed as the ratio like,

$$c_{b,n} = \frac{net\ volume\ of\ species}{net\ volume\ of\ all\ species} \qquad (2.20)$$

And satisfies

$$\sum_{n=1}^{N} c_{b,n} = 1.0 \qquad (2.21)$$

Here, N is for the total number of species. $C_{b,n}$ does not exist in the original Meyer Peter and Muller equation it was added in the equation to account for the effect of multiple species.

# CHAPTER 3

# METHODOLOGY

## 3.1 Introduction

This chapter describes the experimental methodology that used to investigate local scour around a group of bridge piers arranged in a triangular configuration. The study focuses on understanding scour mechanisms, temporal evolution of scour depth, and the effect of pier spacing on scour characteristics. The experimental setup, sediment properties, and data collection procedures are described in detail to ensure reproducibility and reliability of results.

## 3.2 Physical Set-up Data Preparation

The research study was conducted in the Hydraulic Laboratory of the Civil Engineering Department at Zakir Hussain College of Engineering & Technology, Aligarh Muslim University, India (Anand & Beg, 2024). Whereas the collected experimental data from one of the models that will later be used for numerical simulations using Flow-3D software to validate model's findings. Then to carry out simulations on the group of three piers set in a triangular configuration. The experimental was conducted 6 various models of bridge piers. The pier diameter was 4 cm in all cases. The singular bridge pier used in the experimental work as reference model. Later in CFD simulation will used as calibration model to validate the model results with the numerical calibration model that called as Model 0. The measurements of a recirculating rectangular tilting flume were 11 m in length, 0.756 m in width and 0.55 m depth. An overhead tank had a constant head of 5.06 m from the channel's bottom to the tank's water surface. This tank delivered water to the laboratory flume, which in turn received water from the laboratory water supply system. An operational valve in the water supply pipeline regulated the flow of water into the flume. The flume included within glass walls and a steel base to ensuring visual access and structural stability. As shown in the flume drawing layout illustration Figure 3.1.

Whereas the flow discharge it was introduced using a constant-discharge system calibrated at 0.0535 $m^3/s$, with a mean flow velocity of 0.59 m/s and an average water flow depth of 12 cm over the sediment bed. The thickness of sediment material layer was leveled to be 20 cm above the solid bed as shown in Figure 3.1.

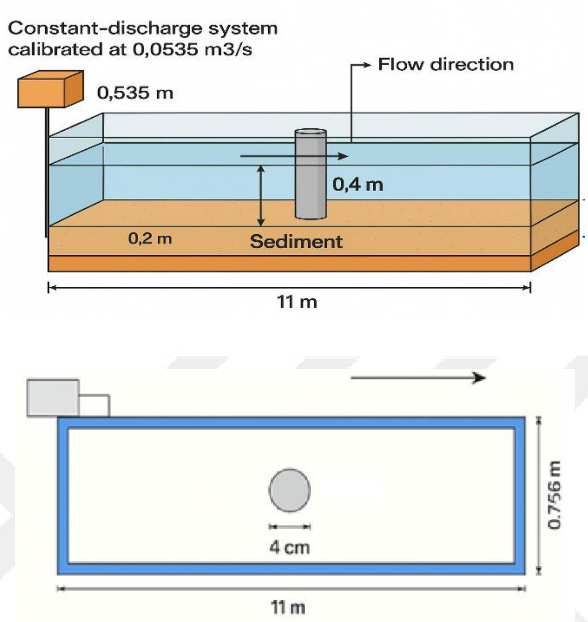


**Figure 3.1** Drawing for illustration of experimental flume layout, geometry and dimensions.

### 3.3 Methodology and Models Scenarios

The methodology is structured into two phases: (1) model calibration using a single pier based on available experimental data, (2) an extended numerical investigation involving pier groups arranged in triangular configurations with various spacing ratios. After the calibration of the numerical model with a single-pier case, five models as of triangular group pier will be simulated to representing one triangular pier group configuration shown in Table 3.1 and Figure 3.2 and Figure 3.3. In this configuration the head forwarding to facing the upstream flow. These five cases are chosen to examine how changes of the pier spacing affect the flow behavior around the group of piers and their influence on local scour depth development. These models differ only in the center-to-center distance between the front and base piers, defined by the non-dimensional ratio Z/b, where Z is the vertical distance between the middle of the base piers line and the head forwarding pier.  and b is the pier diameter (4.0 cm). As shown in Figure 3.2.

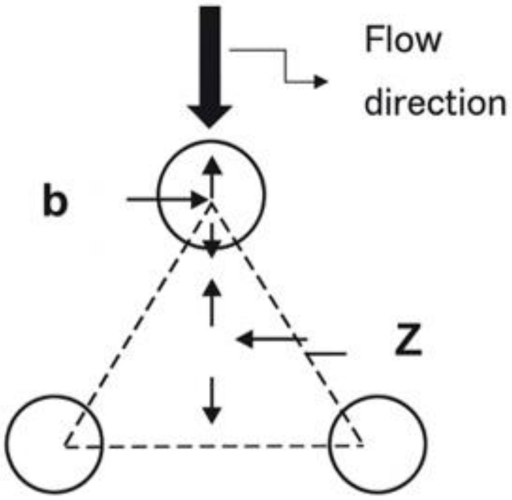


**Figure 3. 2** Illustration of triangular of group of pier configuration.

The selected of Z/b (ranging from 1 to 25) were chosen to reflect a wide range of hydrodynamic interaction scenarios, from strong interference at close spacing to near isolated or isolated behavior at wide spacing as shown in Table 3.1 and Figure 3.3.

**Table 3. 1** Simulation Scenarios

| Model | Z/b Ratio | Z (cm) | b (cm) |
|---|---|---|---|
| Model 0 | - | - | 4 |
| Model 1 | 1.00 | 4.0 | 4 |
| Model 2 | 3.5 | 14.0 | 4 |
| Model 3 | 8.45 | 33.8 | 4 |
| Model 4 | 15.0 | 60.0 | 4 |
| Model 5 | 25.0 | 100.0 | 4 |

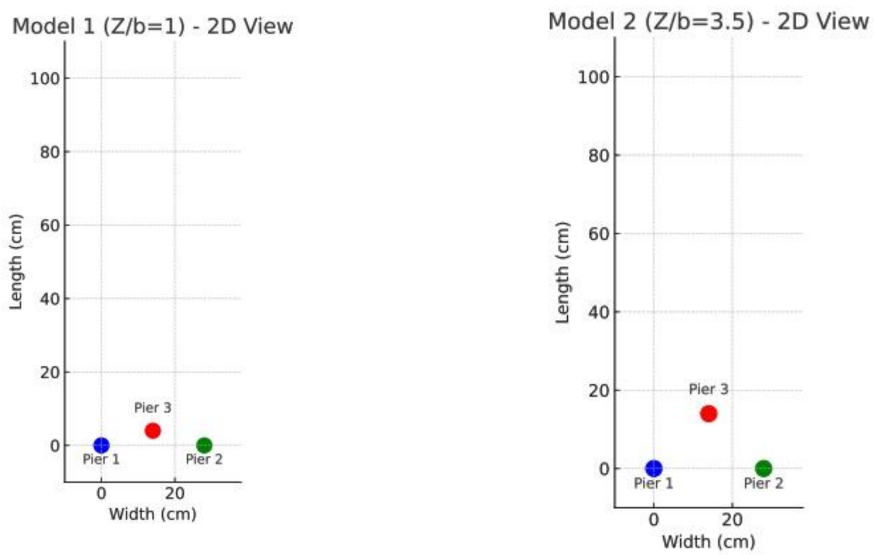

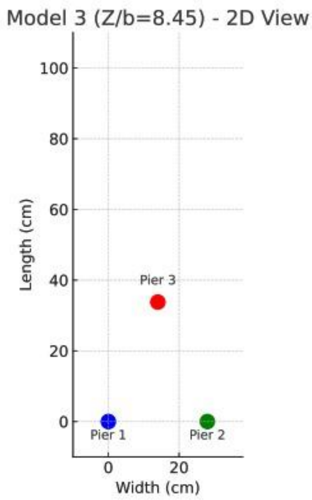


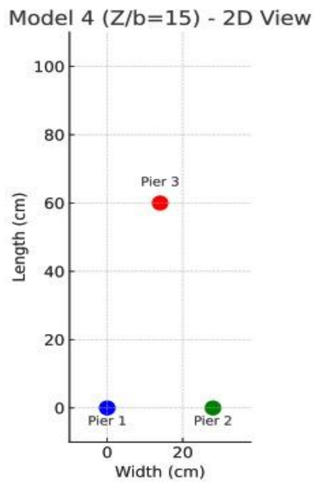


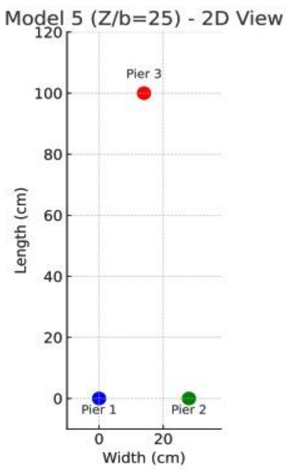


**Figure 3. 3** illustrates of the five model's locations in triangular configuration and Triangular Group Pier Configuration demonstration.

The sediment material flume and flow conditions that used in the experiments and are characterized as shown in Table 3.2 and 3.3:

**Table 3. 2** Flume and Flow Characteristics

| Parameter | Value | Unit |
|---|---|---|
| Flume length | 11.0 | m |
| Flume width | 0.756 | m |
| Water flow depth (h) | 0.12 | m |
| Discharge (Q) | 0.053 | $m^3/s$ |
| Approach velocity (u) | 0.59 | m/s |
| Froude number (Fr) | 0.54 | – |

**Table 3. 3** Characterized sediment material used in the experiments study

| Parameter | Value | Unit |
|---|---|---|
| Median grain size ($d_{50}$) | 3.0 | mm |
| Geometric standard deviation ($\sigma_s$) | 1.2 | – |
| Bed thickness | 0.20 | m |

### 3.3.1 Numerical Modeling with Flow-3D

This study employed the computational fluid dynamics (CFD) software Flow-3D that developed by Flow Science, Inc., for numerical modeling of the scour phenomena. Flow-3D offers robust modules specifically designed for hydraulic engineering investigations. The software utilizes a structured orthogonal grid system combined with the innovative Fractional Area/Volume Obstacle Representation (FAVOR) method, which empowers accurate modeling of complex geometries such as bridge piers without requiring computationally long time and costly consuming for deformed grids. For free surface water flow simulation, Flow-3D implements the Volume-of-Fluid (VOF) method (Hirt & Nichols, 1981), which tracks fluid interaction by calculating the fluid volume fraction in each grid cell. This approach allows the model to maintain sharp air-water boundaries while avoiding the need for excessively fine meshing typically required by other CFD software. The software's capabilities in local scour modeling have been well-documented (Brethour, 2003), making it particularly suitable for this study. Additional features that enhance its effectiveness for hydraulic structure analysis include the implementation of multiple and nested meshes for localized enhancement, as well as a re-run capability that facilitates parametric studies. The FAVOR method's efficient handling of solid boundaries enables the simulation of obstacles like bridge piers within a fully structured grid framework, while the software's ability to account for wet and dry cells ensures computational efficiency by minimizing unnecessary calculations in inactive domain regions. These combined features make Flow-3D an ideal tool for investigating the complex flow dynamics and scour mechanisms around bridge piers.

### 3.3.2 Numerical Methodology

In this study, the methodology of numerical simulation of local scour around cylindrical bridge piers was performed using FLOW-3D, a computational fluid dynamics (CFD) software capable of modeling free-surface flow and sediment transport. There were phases approached in this research methodology as following:

### 3.3.3 Numerical Method Used in FLOW-3D

FLOW-3D employs the Finite Volume Method (FVM) to solve the three-dimensional, transient Navier–Stokes equations that govern fluid motion. The equations are discretized over a structured Cartesian mesh, allowing accurate representation of flow parameters in each control volume.

### 3.3.4 FAVOR Method

In this study, FLOW-3D, developed by Flow Science Inc., was utilized for numerical modeling. This commercial CFD software is widely applied in hydraulic engineering due to its robust modules for simulating complex flow behaviors. FLOW-3D employs a structured Cartesian mesh and the Fractional Area/Volume Obstacle Representation (FAVOR) method to accurately model intricate geometries such as bridge piers. The Volume of Fluid (VOF) technique (Hirt and Nichols, 1981) is used to capture the free-surface interface between water and air, allowing precise tracking of fluid boundaries without requiring excessively fine meshes. The software effectively models local scour phenomena (Brethour, 2001) and represents solid obstacles through fractional volumes and face areas within each grid cell. Additional features, such as multiple and nested mesh capabilities and re-run options, enhance its flexibility in hydraulic simulations. Compared to other CFD tools that require body-fitted or deformed meshes, FLOW-3D's FAVOR method efficiently handles wetting and drying processes while maintaining numerical stability and computational efficiency.

The FAVOR method is chosen because:

- It accurately models complex pier geometries without the need for body-fitted grids.
- It ensures mass conservation and numerical stability in multiphase free-surface flows.
- It is computationally efficient, ideal for long-duration scour simulations.
- It reduces numerical diffusion compared to immersed-boundary or cut-cell methods.

Other methods available in FLOW-3D include TruVOF (for free-surface tracking), Porosity-based methods, and General Moving Object (GMO) modeling. However, FAVOR provides the best balance between accuracy and computational simplicity for fixed bridge pier structures.

### 3.3.5 FLOW-3D Model Set-Up and Calibration

To support and extend the experimental investigation, numerical simulations were carried out using FLOW-3D, a computational fluid dynamics (CFD) software specifically designed for modeling free-surface flows and sediment transport. The numerical modeling aimed to simulate the experimental single-pier namely Model (0) case for validation, then analyze scour behavior around triangular pier group configurations.

### 3.3.6 Physics Configuration

Flow-3D offers comprehensive physics modeling capabilities essential for scour simulation, including sediment transport, scour analysis, and other critical hydrodynamic processes. The key physics modules activated for this study include Sediment scour modeling, Gravity and non-inertial reference frame, Fluid viscosity, Turbulence effects. Each physics module contains multiple sub-options that can be fine-tuned to match specific simulation requirements.

### 3.3.7 Gravity and Density

The gravitational acceleration was set to -9.81 $m/s^2$ in the vertical direction Z as shown in Figure 3. 1to accurately represent real-world conditions. Also, the software calculates fluid density as a function of several variables.

### 3.3.8 Model Geometry

The computational domain was designed to closely match the experimental flume setup. The sediment bed was modeled as 3 meters as section work needs within the flume and thickness of 0.2 meter. A vertical cylindrical pier with a diameter of 4 cm and a height of 0.5 m was placed at -0.2 m of the sediment bed.

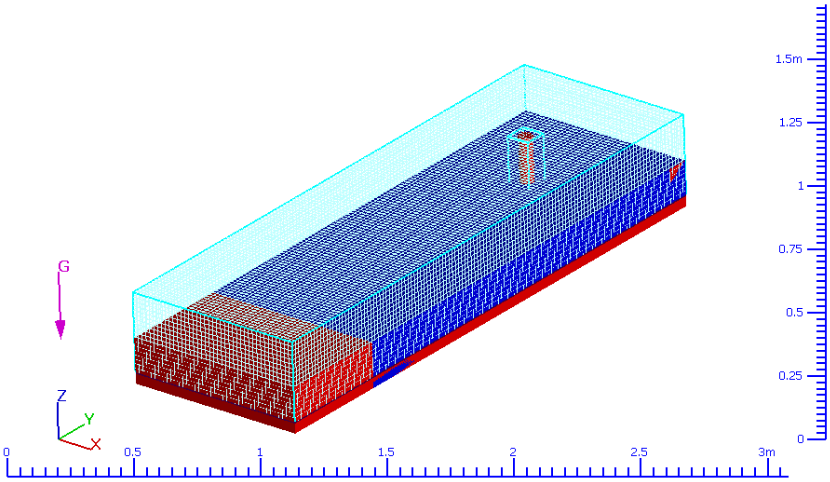


**Figure 3. 4** Model Geometry

### 3.3.9 Mesh

A uniform mesh was used in the simulation in two layers, with a grid size of 2 cm in all directions as well as intensify the mesh around the pier with 1 cm. These meshes resulted in a total of approximately 128,000 cells. The chosen mesh was fine enough to capture detailed flow features such as vortex formation and shear stress distributions while keeping the computational cost within practical limits.

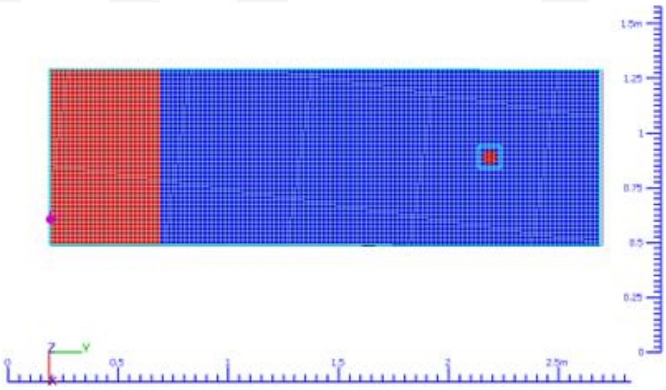

**Figure 3. 5** Mesh and Resolution

### 3.3.10 Boundary and Initial Conditions

The flow entered the domain from the upstream side as shown in Figure 3.6 the discharge inlet (Q), with a discharge 0.053 $m^3/s$. The outlet at the downstream end was set as outlet to allow free flow out discharge (O). The sidewalls of the flume (in the X-direction) were modeled with no-slip wall conditions to represent solid channel boundaries (S). The bottom of the domain was also set as a fixed no-slip wall to replicate the physical bed. The top surface was considered as a pressure boundary to simulate free water surface in open-channel flow. The initial water depth was set to be 12 cm above the sediment bed.

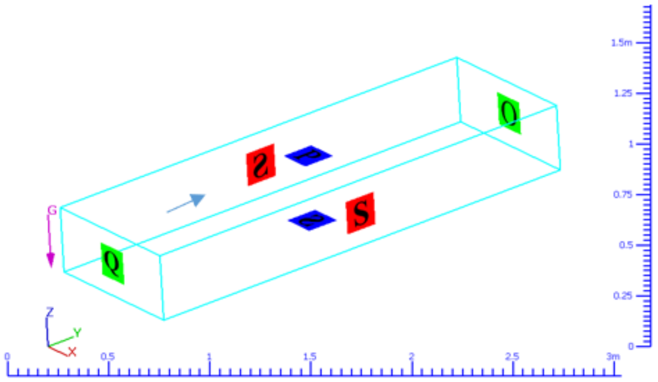


**Figure 3. 6** Boundary and Initial Conditions

### 3.3.11 Sediment Modeling and Properties

The sediment bed was modeled as a non-cohesive layer with a median diameter of 3 mm and a specific gravity of 2.65. The bulk density of the sediment was taken as 2650 $kg/m^3$. Both bedload and sediment transport were activated in the model to fully represent sediment dynamics during scour formation.

## 3.4 Model Calibration

The numerical simulations in FLOW-3D were performed to calibrate the numerical model with the experimental results for a singular cylindrical bridge pier this model will be mentioned as Model 0. The domain dimensions matched the laboratory flume (11.0 m × 0.756 m × 0.55 m) with a 0.20 m sediment layer and an average flow depth of 0.12 m. Flow was imposed at a discharge of 0.0535 $m^3/s$, corresponding to a mean velocity of 0.59 m/s, while the pier was modeled as a cylinder (0.04 m diameter) placed at the solid bed channel.

Sediment parameters included a median grain size ($d_{50}$) of 0.003 m, density 2650 $kg/m^3$, and a critical packing fraction of 0.64, with transport controlled by an entrainment coefficient of 0.018, bed load coefficient of 12, and an angle of repose of 32°. The computational grid (0.01–0.02 m) and run duration (120 min) were selected to capture equilibrium scour. The complete run conditions are summarized in Table 3.3. The calibration depends on sediment and flow parameters reliable with the experimental conditions. Specifically, the critical Shields parameter was calculated by

Soulsby-Whitehouse equation, and Nielson equation were used for bed load of sediment transportation rate. These parameters are summarized in Table 3.4.

**Table 3. 4** Numerical Run Conditions for CFD Simulations

| Parameter | Value | Notes |
|---|---|---|
| Length (m) | 11.0 | Same as experimental flume |
| Width (m) | 0.756 | Same as experimental flume |
| Depth (m) | 0.55 | Same as experimental flume |
| Sediment Layer Thickness (m) | 0.20 | Loose sediment placed above steel bed |
| Water Flow Depth (m) | 0.12 | Average depth over sediment layer |
| Discharge ($m^3$/s) | 0.0535 | Constant-discharge inlet condition |
| Mean Flow Velocity (m/s) | 0.59 | Depth-averaged velocity |
| Pier Diameter (m) | 0.04 | For single and grouped pier models |
| Pier Height (m) | 0.40 | Extending above sediment and water depth |
| Grain Size, $d_{50}$ (m) | 0.003 | Uniform sediment size |
| Sediment Density (kg/$m^3$) | 2650 | |
| Critical Packing Fraction | 0.64 | As defined in sediment model |
| Critical Shields Parameter | Calculated automatically by Flow 3d through Soulsby-Whitehouse equation | |
| Bed Roughness / $d_{50}$ Ratio | 2.5 | Roughness scaled to sediment size |
| Entrainment Coefficient | 0.018 | Sediment transport parameter |
| Bed Load Coefficient | 12 | Empirical transport factor |

The calibration of the numerical model was initially carried out for the singular cylindrical bridge pier (Model 0) in order to ensure the reliability of the CFD setup prior to extending the analysis to grouped pier configurations. The comparison between the physical measurements and the CFD predictions revealed a strong agreement, demonstrating that the model is capable of reproducing the temporal and spatial development of local scour observed in the laboratory.

As shown in Figure 3.7, the relationship between the experimental (EXP) and numerical (CFD) results showed a nearly one-to-one correspondence across the different recorded time intervals. This indicates that the CFD model successfully captured the governing hydraulic and sediment transport processes. $R^2 = 0.97$ confirms the reliability of the calibration, reflecting that approximately 97% of the variability in the experimental results was explained by the numerical model. Such a high level of correlation validates the numerical assumptions and parameterization adopted in the simulations, including sediment transport coefficients, bed roughness scaling, and Shields parameter calculations.

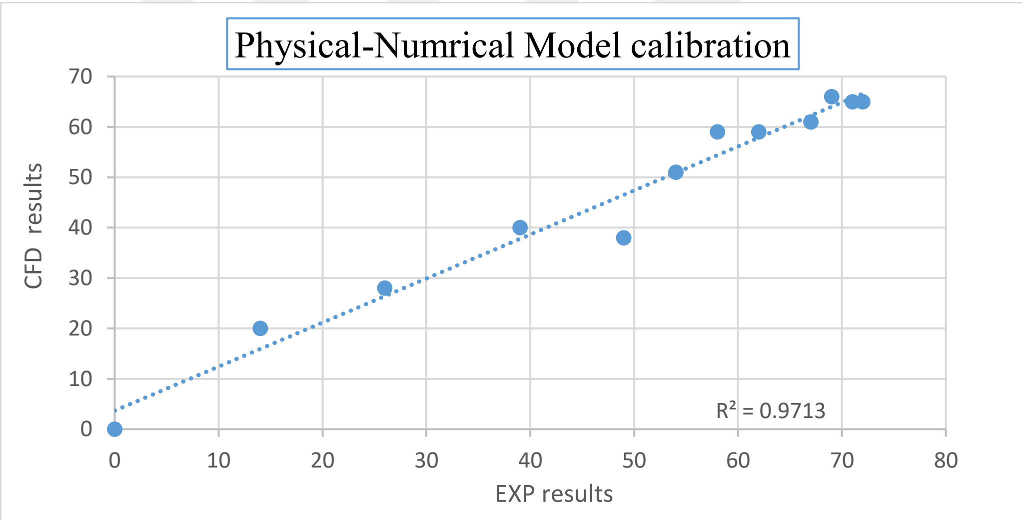


**Figure 3. 7** Experimental and Numerical Model (Model 0) Calibration.

The successful calibration for the single pier provides a solid basis for extending the numerical study to more complex pier arrangements, such as triangular and staggered configurations. Moreover, it confirms that FLOW-3D, when properly calibrated, can serve as a reliable predictive tool for simulating scour phenomena under laboratory and potentially field-scale conditions.

In this configuration the head forwarding to facing the upstream flow. These five cases are chosen to examine how changes of the pier spacing affect the flow behavior around the group of piers and their influence on local scour depth development as shown in and Figure 3.8. All model simulations are conducted under the same flow and sediment conditions as the validated experimental setup, including identical flow discharge, water depth, and sediment properties. This consistency ensures that any differences in scour behavior can be attributed only to the pier spacing, rather than changes in hydraulic conditions

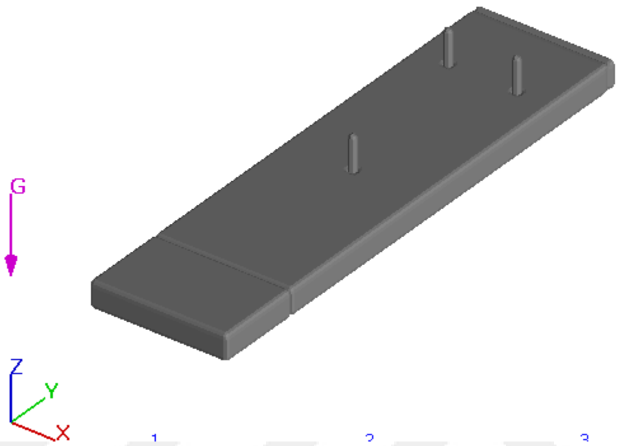


**Figure 3. 8** CFD illustrated of triangular configuration in Z/b=25 in case

# CHAPTER 4

# RESULTS AND DISCUSSION

## 4.1 Introduction

This chapter presents the results of computational simulations conducted to investigate local scour behavior around triangular bridge pier configurations. The models were performed using the FLOW-3D software after successful calibration of the model with a single cylindrical pier, which was compared with an experimental study in the same conditions, referred to as Model 0, and used as a reference case to validate the model's performance. This research focuses on five additional models (models 1 to model 5) representing a forward-facing triangular pier group configuration, where the triangle points upstream in the direction of the flow. These models differ only in the center-to-center distance between the front and base piers, defined by the non-dimensional ratio Z/b, where Z is the spacing distance and b is the pier diameter (4.0 cm). The selected values of Z/b (ranging from 1.00 to 25.00) were chosen to reflect a wide range of hydrodynamic interaction scenarios, from strong interference at close spacing to near-isolated behavior at wide spacing. All simulations were conducted under the same flow discharge, sediment characteristics, and flume geometry to ensure that any variation in the results is only due to changes in pier spacing. The results are evaluated through multiple approaches, including velocity field analysis, Scour hole shape (2D and 3D bed deformation), developments of scour depth with time, and comparative assessment.

## 4.2 Results of model's Z/b=1 to Z/b =25

This section presents the numerical results obtained from the triangular grouped pier configurations with a spacing ratio of Z/b = from 1 to 25. In this arrangement, the three cylindrical piers are arranged in a forward-facing triangular formation, where the vertex pier directly confronts the incoming flow, and the two rear piers are aligned symmetrically downstream.

The aim is to understand the effect of pier spacing (Z/b ratio) on scour depth, flow field characteristics, bed morphology, and the temporal evolution of scour.

### 4.3 Results of Triangular Grouped Pier Model – Z/b = 1.0

#### 4.3.1 Flow Dynamics and Velocity Field

In the Model 1 configuration, the spacing ratio between the front and rear piers was Z/b = 1.0. The velocity field indicates localized acceleration near the front pier, accompanied by flow contraction between the configuration of triangular grouped bridge piers. This encourages the development of high-intensity horseshoe vortices and wake turbulence, which enhance the sediment transport capacity around the triangular grouped bridge piers. As shown in Figure 1. Upon entering the upstream region, the flow encounters the front pier head-on, causing a sharp deceleration immediately in front of the pier and forcing water around its sides. This redirection of flow accelerates the velocity in the narrow openings between the front and base piers. Because the spacing is at minimal, these gaps act as flow constriction channels, producing jet-like acceleration zones that further increase shear stress on the bed. Also, intensifies the horseshoe vortices at the upstream pier and increasing the vortex that coming between and behind the piers.

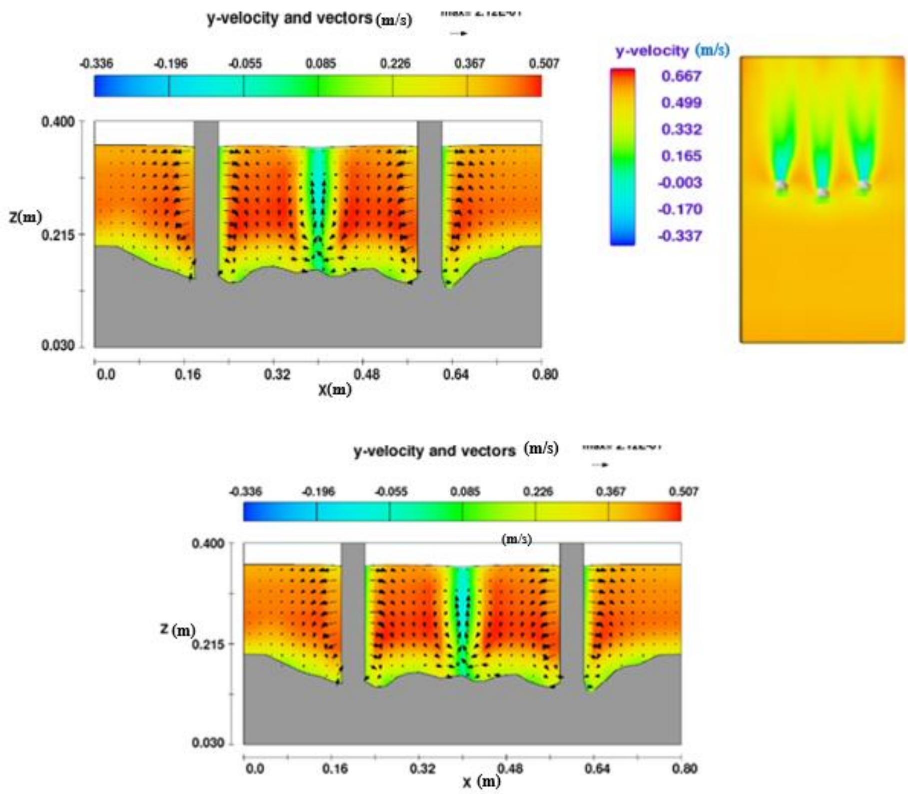


**Figure 4. 1** The localized acceleration velocity field around the front and rear piers

Furthermore, the velocity field in Figure 4.1 clearly shows concentrated high-velocity streaks between the piers. These high-energy jets feed into the wake region, where large-scale turbulence dominates. Immediately at the base of the front pier, a strong horseshoe vortex system forms, wrapping around the pier and scouring sediment from its base. Behind the front pier, the wake interacts almost instantly with the two rear piers, producing secondary horseshoe vortices and wake vortices that intensify sediment removal around them.

### 4.3.2 Deformation of Bed Morphology – 2D and 3D Perspective

Figure 4.2 (a and b) shows the bed elevation contour maps and three-dimensional deformation of the bed the colored bars show that in the Z/b configuration, the scour hole around the front pier reached a maximum depth of 100.5 mm The rear piers experienced an average scour depth of 95.5 mm. The scour pattern varies from highly merged and symmetric at low spacing. The bed elevation contour map as shown in Figure 4.2a. reveals that the scour holes around the three piers have fully merged into one continuous depression. This merging indicates that there is no stable recovery zone between the piers where sediment could settle down so the turbulence from the front pier feeds directly into the erosion zones of the rear piers.

Also as shown Figure 4.2 (b) the front pier experienced the greatest scour depth at 100.5 mm. This is attributed to the high concentration of flow energy and intense horseshoe vortex formation at the leading pier. The rear piers also showed significant scour depths (94 mm and 97 mm), indicating strong vortex interaction and limited space for flow dissipation. The scour holes merged considerably, resulting in a high negative interaction depth of -53 mm, closeness scour hole overlap as shown in Figure 4.2 (a).

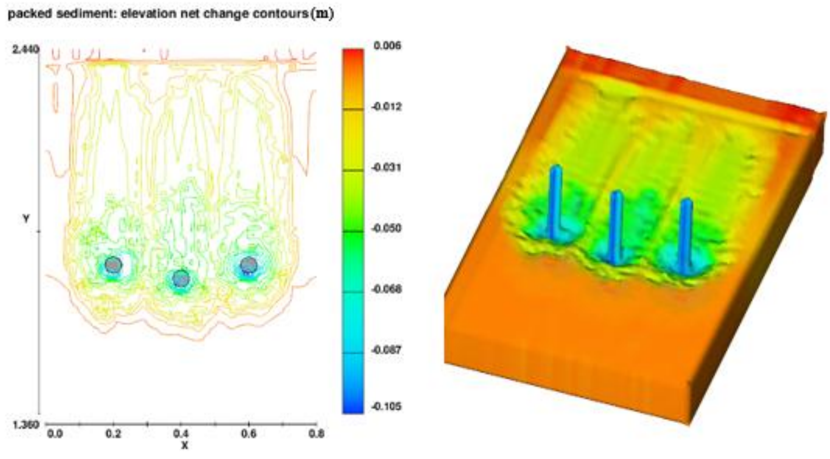


a b

**Figure 4. 2**. (a) The bed elevation contour maps (b) 3D Bed Deformation.

### 4.3.3 Development of Scour with Time

Figure 4.3 illustrated the time-scour developments of scour depth which reveals that scour is most intense during the first half hours of simulation in this case. The rate of scour stabilizes as the sediment transport reaches equilibrium. These dynamic trends provide insight into the temporal vulnerability of pier foundations during flood events or sustained high-flow conditions.

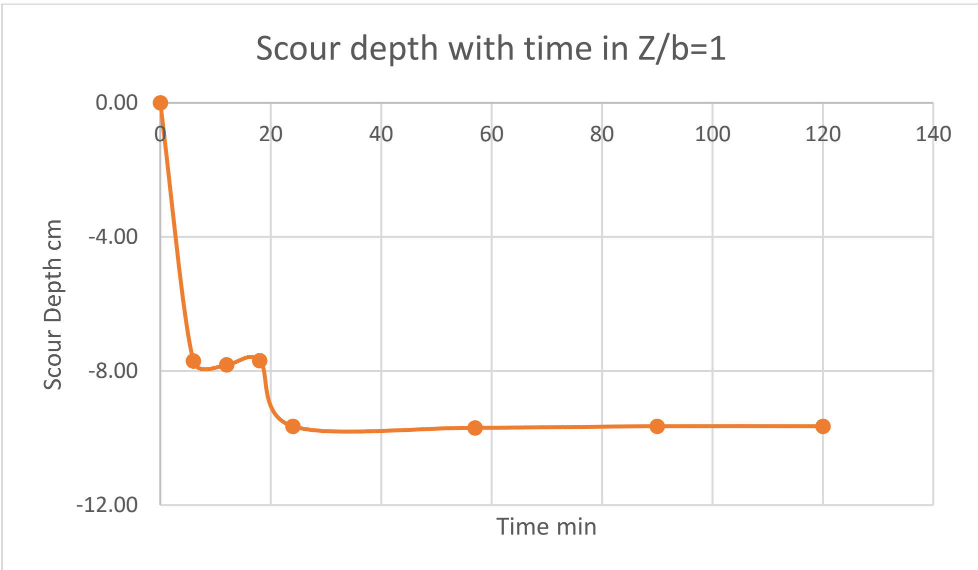


**Figure 4. 3** Illustration scours developments with time of local scour depth

The Z/b = 1.0 configuration represents the closest possible spacing between the front (apex) pier and the two downstream base piers in the triangular arrangement. This extremely tight arrangement creates a single, highly interactive hydraulic zone, where the three piers act collectively as a compound obstruction to the flow.

### 4.4 Results of Triangular Grouped Pier Model (Z/b = 3.5).

In the Z/b = 3.5 configuration, the spacing between the front pier and the rear base piers is increased compared to the previous case, providing wider flow passages and slightly more area for hydrodynamic recovery. However, the piers remain close enough for significant interaction between their respective flow fields and scour zones.

#### 4.4.1 Flow Dynamics and Velocity Field for Model (Z/b = 3.5).

As the incoming flow meets the front pier and still experiences direct stagnation pressure at the face of front pier, producing a strong horseshoe vortex at its base. The flow is then deflected laterally into the two side of the pier, where the flow accelerates due to the reduced cross-sectional area. The contraction effect is less severe when compared to Z/b = 1.0, which reduces the intensity of the jet-like flows entering the wake zone. However, as shown in Figure 4.4 the velocity field map shows that high-velocity streaks continue along the paths leading to the rear piers, delivering enough kinetic energy to generate secondary horseshoe vortices at their bases. The wake region behind the front pier is more diffuse than in the tighter spacing case, but still overlaps with the downstream piers' approach zones. This overlap maintains a turbulent connection between the piers, preventing complete hydraulic independence.

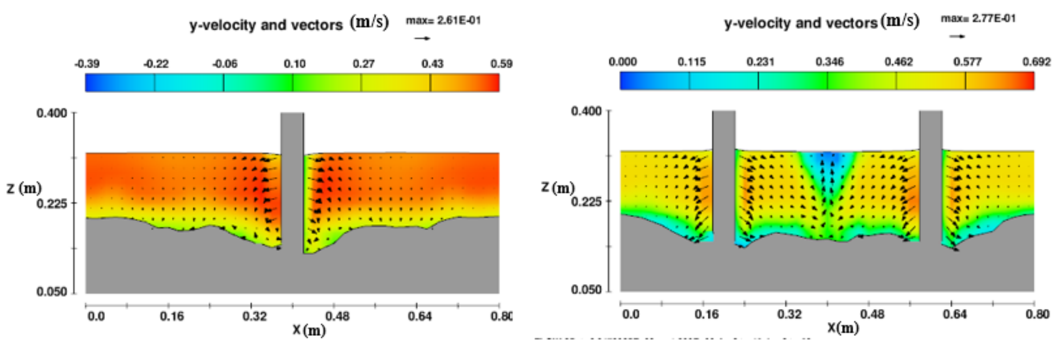

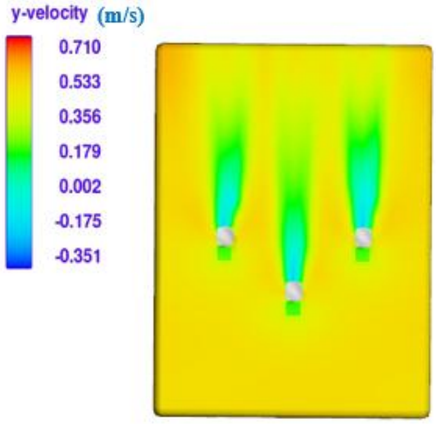


**Figure 4. 4** The localized acceleration velocity field around the front and rear piers.

### 4.4.2 Deformation of Bed Morphology – 2D and 3D Perspective

The bed elevation contours reveal in Figure 4. 5 (a) that the scour holes are partially merged, with a continuous but shallower connecting trough between the front and rear piers. The maximum scour depth at the front pier decreased to 92.2 mm, while the rear piers recorded depths of approximately 78 mm and 81.1 mm. Also, Figure 4. 5 (b) shown that the 3D bed profile demonstrations a central deep zone at the front pier, surrounding by two moderately deep depressions at the rear piers. The connecting scour trough is shallower than in Z/b = 1.0, indicating some reduction in energy transfer between the vortices of different piers.

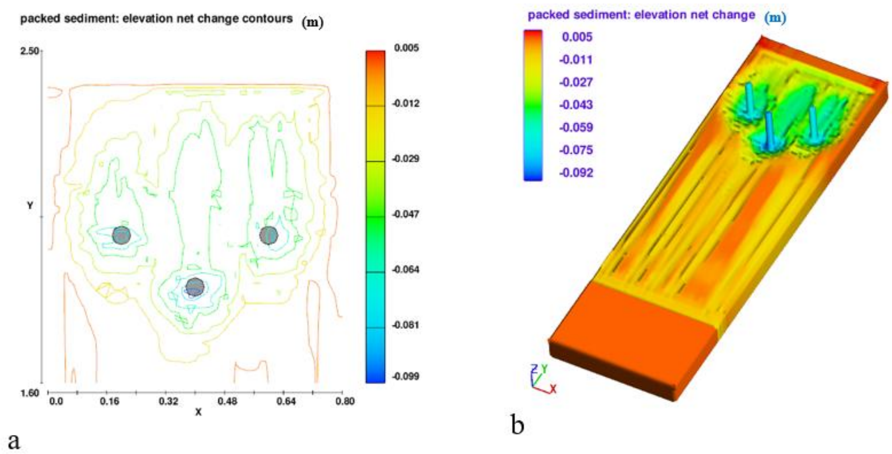


**Figure 4. 5** (a) The bed elevation contour maps (b) 3D Bed Deformation.

From Figure 4. 5 (a) contour plots of the bed elevation illustrate the spatial extent of scour holes around the piers. The front pier consistently experiences the highest scour depth due to direct flow impact. The rear piers, although somewhat shielded, still show notable erosion due to redirected flows and turbulent interactions. In Figure 4. 5 (b) expressions that the three-dimensional deformation profiles further confirm the formation of well-developed scour holes, especially under low Z/b ratios. As the spacing increases, flow interference reduces, and the scour morphology begins to resemble that of isolated piers.

### 4.4.3 Development of Scour with Time

The time-series plot indicates a rapid initial deepening phase within the first 10 – 15 minutes, after which the rate of scour slows and approaches equilibrium after 50-60 minutes. The slower approach to the asymptotic scour depth compared to Z/b = 1.0 reflects the slightly weaker initial vortex intensity due to reduced flow contraction.

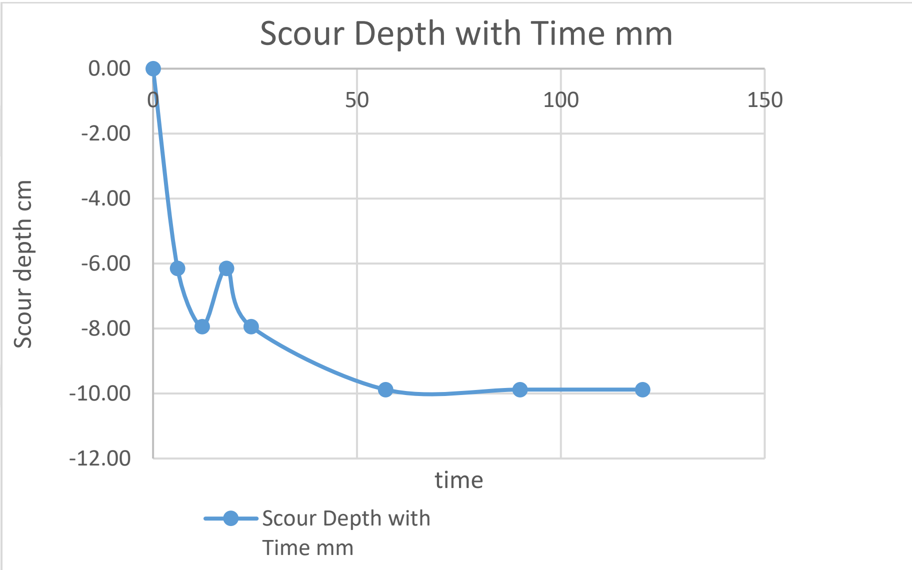


**Figure 4. 6** Illustration of scours depth developments with time Z/b =3.5

## 4.5 Results of Triangular Grouped Pier Model (Z/b = 8.45).

In the Z/b = 8.45 configuration, the spacing between the front pier and the rear base piers is more than double that of the previous case. This wider separation allows the flow more distance to redistribute after passing the front pier, significantly reducing direct hydraulic interference.

### 4.5.1 Flow Dynamics and Velocity Field

Upon striking the front pier by the incoming flow generates a prominent horseshoe vortex at its base due to stagnation and flow separation Figure 4.7. However, the larger opening area between piers gives the accelerated flow into two sides enough space to expand and redistribute energy before reaching the rear piers. The velocity field map shows that high-velocity regions are now more localized around each pier, with only partial overlap between the front pier's wake and the rear piers' approach flows.

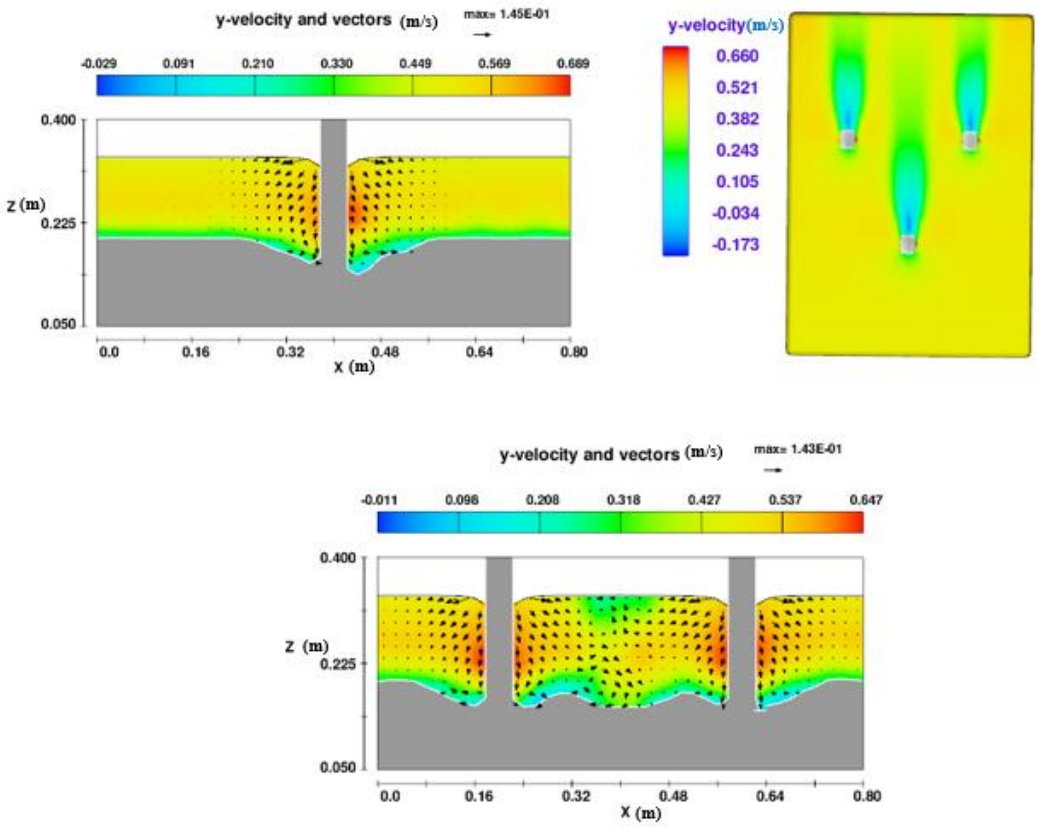


**Figure 4. 7** Flow Dynamics and Velocity Field

This reduction in overlap means that wake turbulence from the front pier no longer dominates the hydrodynamics at the rear piers. Although contraction effects remain present near the side gaps, they are considerably weaker, leading to less intense shear stress on the sediment bed in the inter-pier region.

### 4.5.2 Deformation of Bed Morphology – 2D and 3D Perspective

The bed elevation contours shown in Figure 4. 8 (a) The bed elevation contours reveal that scour holes are now distinctly more separated compared to the previous cases. The maximum scour depth at the front pier dropped to 88.0 mm, while the rear piers experienced substantially lower scour depths of 69.7 mm and 69.3 mm. The 3D bed profile in Figure 4. 8 (b) confirms this separation, showing three individual scour depressions with only shallow linking troughs. The shapes of these holes are more elongated in the downstream direction, reflecting a reduced influence from neighboring piers and a stronger alignment with the local flow path.

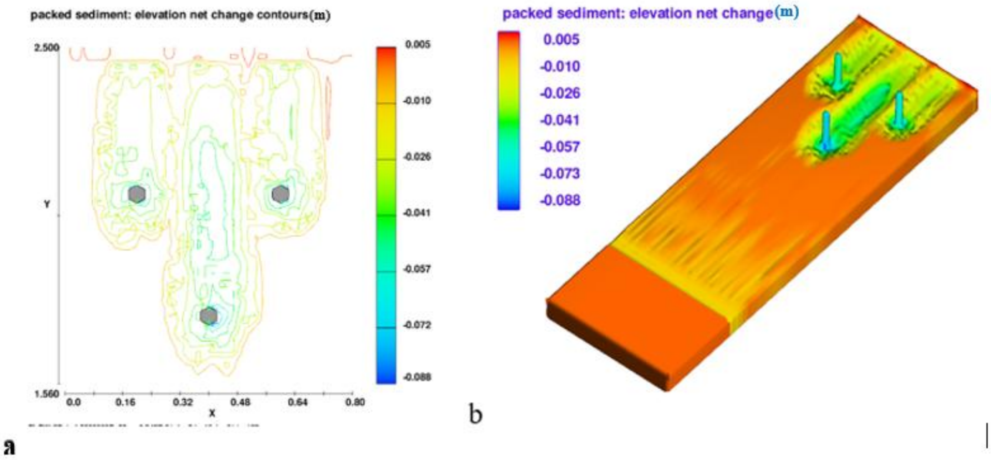


**Figure 4. 8** (a)The bed elevation contour maps (b) 3D Bed Deformation.

### 4.5.3 Development of Scour with Time

The time-series plot shows a moderate initial slope compared to both Z/b = 1.0 and Z/b = 3.5, meaning that scour develops more gradually. The front pier still experiences faster early-stage deepening than the rear piers, but all three reach their equilibrium depths at a slower rate overall.

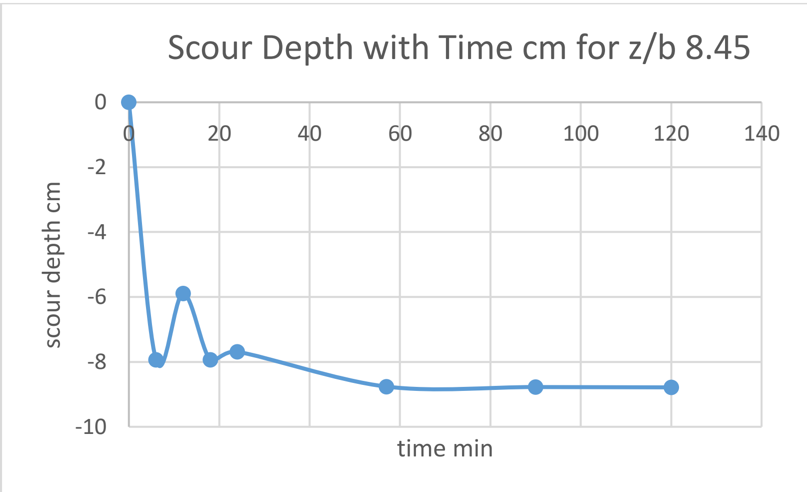


**Figure 4. 9** Illustration of scours depth developments with time z/b =3.5

## 4.6 Results of Triangular Grouped Pier Model (Z/b = 15).

The Z/b = 15 configuration represents a point in the series where the separation between the front pier and the downstream base piers is sufficiently large to allow substantial flow recovery. In hydraulic terms, the flow exiting the front pier wake has enough physical space to dissipate a considerable portion of its kinetic energy before encountering the downstream piers. This case marks a transition toward quasi -isolated (almost isolated) pier behavior, where interaction effects still exist but are no longer the dominant factor controlling scour morphology.

### 4.6.1 Flow Dynamics and Velocity Field

As the approaching flow reaches the front pier, it still experiences a stagnation zone directly upstream, resulting in the formation of a strong primary horseshoe vortex at the pier base. Flow separation along the pier sides generates lateral flow acceleration (jets) that expand into the inter-piers region. With a Z/b of 15, these flow accelerations have a wider space to disperse, significantly reducing the magnitude of acceleration zones downstream.

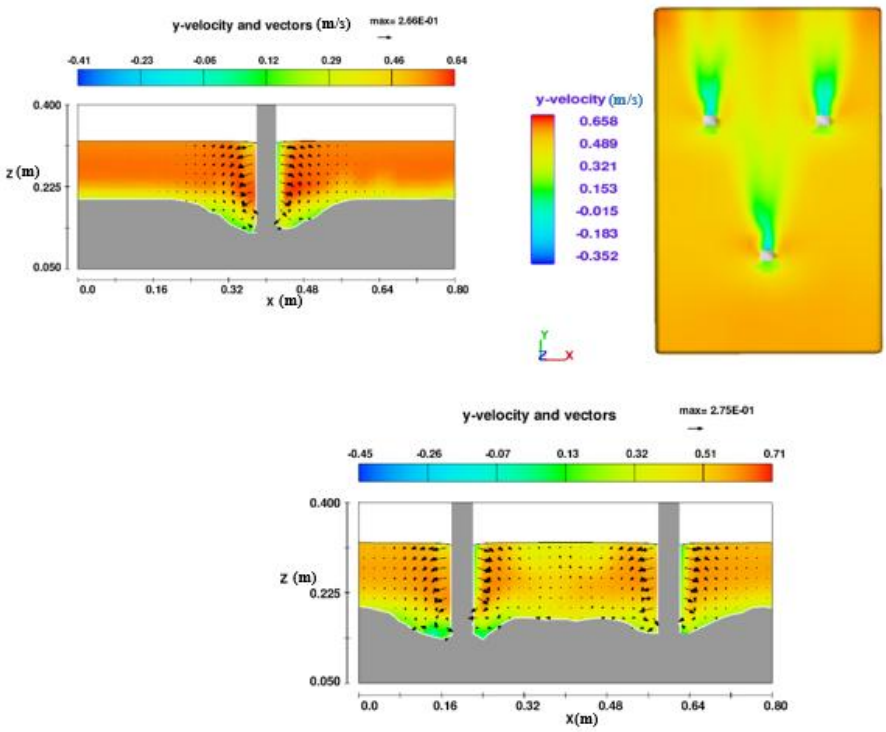


**Figure 4. 10** Flow Dynamics and Velocity Field

### 4.6.2 Deformation of Bed Morphology – 2D and 3D Perspective

The bed elevation contours shown in figure 11 (a-b) depict three distinct scour holes with minimal contour elevation interaction a. The front pier recorded a maximum scour depth of 92.4 mm, while the rear piers exhibit depths of 80.9 mm and 77.9 mm. These values confirm the diminished influence of the front pier on the scour development at the rear piers. Also, the 3D bed deformation profile shown in figure 11 (b) tells that scour holes are symmetric in shape, with well-defined edges and shallower slopes than those seen in closely spaced configurations. The separation between the holes indicates that sediment transport in the wake of the front pier is insufficient to cause bed lowering in the vicinity of the rear piers, meaning their scour is primarily driven by their own local approach flows.

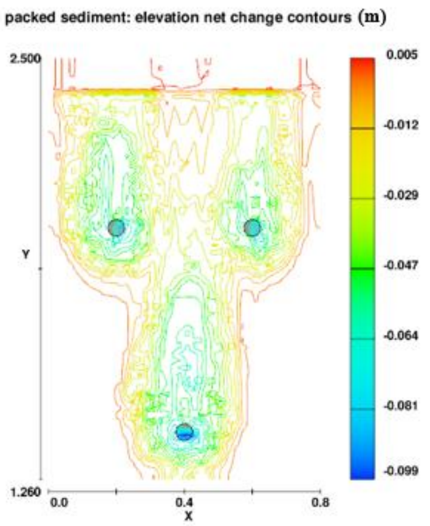


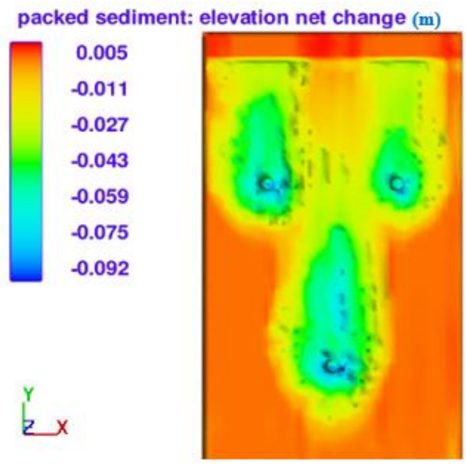


b

**Figure 4. 11** (a)The bed elevation contour maps (b) 3D Bed Deformation

### 4.6.3 Development of Scour with Time

The scour time-series plot for Z/b = 15 shows in figure 4.22 a moderately rapid initial deepening for the front pier during the first 40 min in the first phase , after 50 min the scour depth starts to be stable and by the end time equilibrium is reached, the depths are substantially lower than those in high-interference cases, and the growth curves flatten prior for the rear piers than for the front pier.

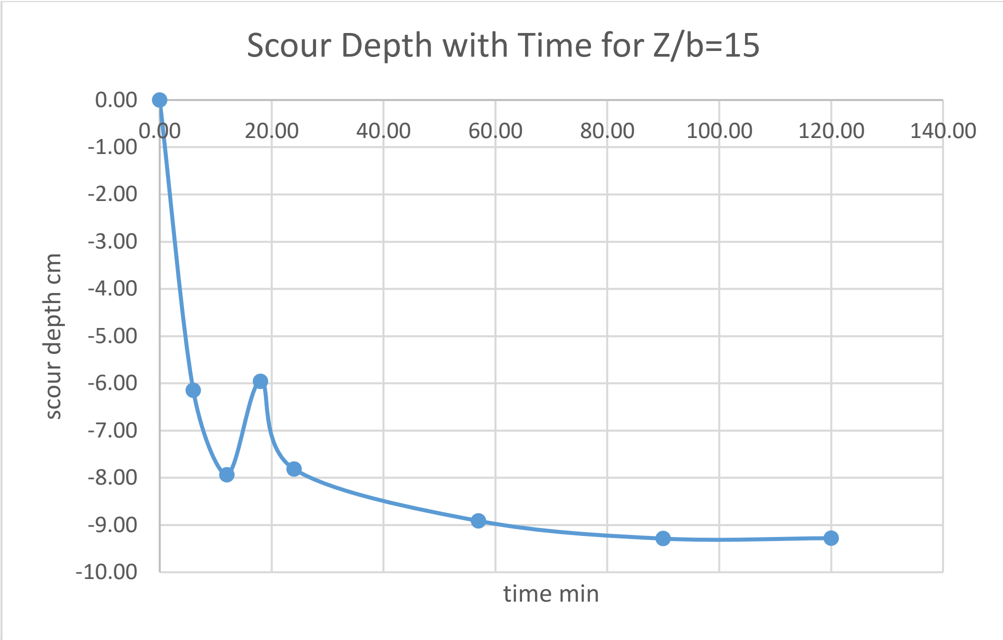


**Figure 4. 12** Illustration of scours depth developments with time Z/b =15.

### 4.7 Results of Triangular Grouped Pier Model (Z/b= 25).

The Z/b = 25 arrangement is the widest spacing tested in this study and represents a scenario where the piers behave as completely hydrodynamically independent structures. At this separation, there is no measurable overlap of wakes or approach zones, and scour development at each pier is governed solely by its own localized flow conditions.

#### 4.7.1 Flow Dynamics and Velocity Field

In this configuration, the incoming flow attacks each pier individually, producing separate stagnation zones and isolated horseshoe vortices. The velocity field confirms that acceleration zones remain confined to the immediate and close vicinity (zone) of each pier and do not extend toward other piers. Also figures shown that there is no noticeable overlap of wakes or approach zones at this intervention, and each pier's scour development is entirely controlled by its own localized flow circumstances. For the front pier, the wake develops fully and dissipates well before reaching the downstream piers, while the rear piers generate their own vortices and wakes independently. The absence of shared contraction passages between the piers eliminates any compounded acceleration or turbulence effects As a result, bed shear stresses in the mid-channel space between piers are minimal, which is clearly noticed in Figure 4. 13.

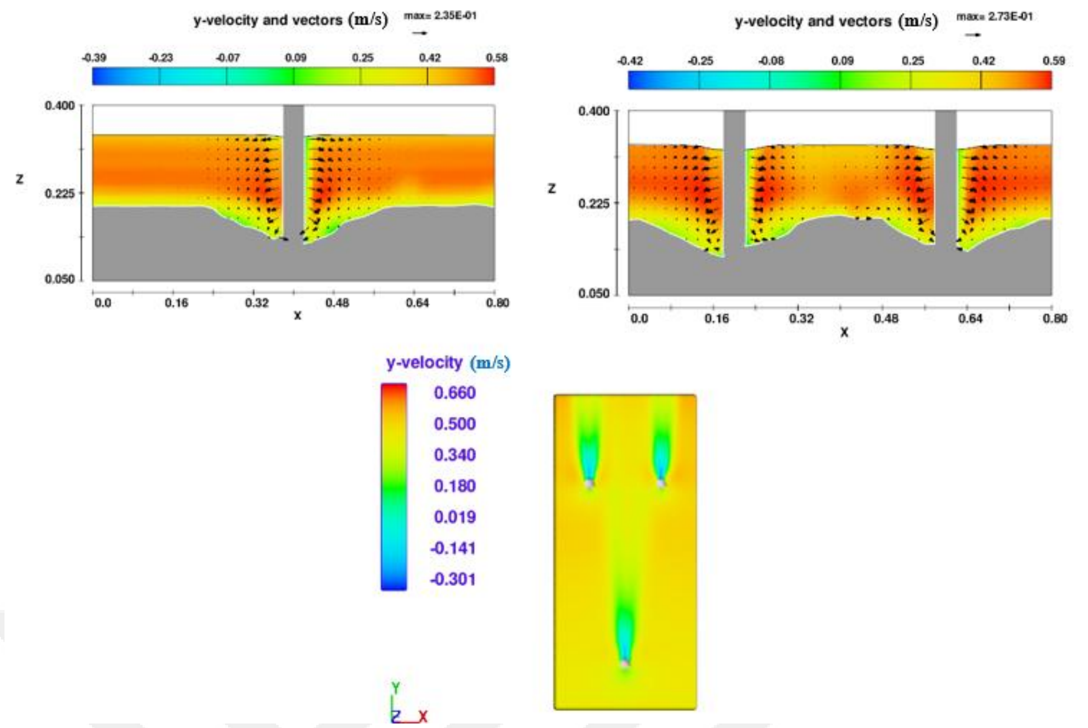


**Figure 4. 13** Flow Dynamics and Velocity Field.

### 4.7.2 Deformation of Bed Morphology – 2D and 3D Perspective

In this model the bed elevation contours for Z/b = 25 as illustrated in figure 4.14 (a and b) show fully separated scour holes. Interestingly, the maximum scour depth at the front pier is 96.1 mm while in 3D Bed Deformation figure 4.14 b the max scour depth is 92 mm in same pier, the deference maybe can be referred it the accuracy of contours line on mesh size, while the rear piers reach 90 mm and 92 mm.

The front pier showed a significant scour depth, and both rear piers displayed high but symmetrical values. This suggests that each pier behaved as an independent structure in the flow field, with negligible interference effects. Also,This relatively high scour at one of the rear piers suggests that local flow patterns, as minor asymmetries in velocity distribution or secondary channeling, can sometimes produce scour depths that rival or exceed those at the front pier. The 3D bed profiles display smooth, symmetric depressions with steep slopes immediately adjacent to the piers but without any interconnecting erosional features. Each scour hole is aligned with the local approach velocity direction, reinforcing the independence of hydrodynamic action at each pier. In addition, the intervention ware positive which refers to non-intervention can be seen clearly in Figure 14 (b)

In another meaning the front pier's effects on the rear piers is terminated due to spacing, which allows the local scour affects around each pier to work separately without receiving enough influence from the anther pier that led to effect on it.

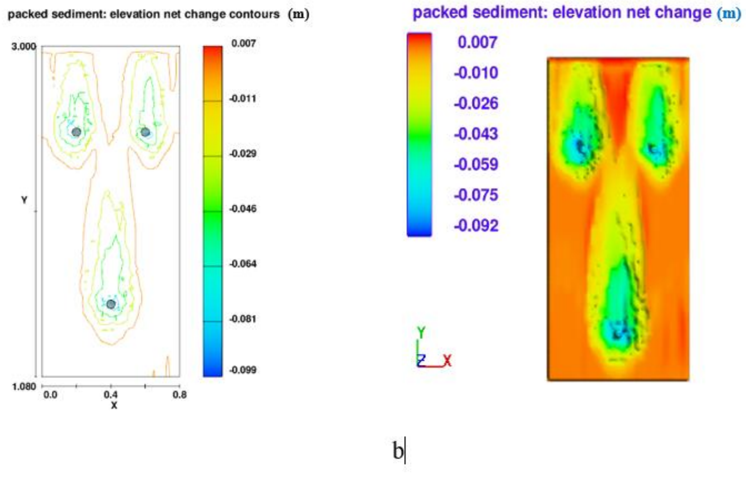


**Figure 4. 14** (a)The bed elevation contour maps (b) 3D Bed Deformation.

### 4.7.3 Development of Scour with Time

The time-series curves in Figure 4. 15 for all three piers in the Z/b = 25 configuration are remarkably similar in shape and slope. The scour process begins with a rapid initiation phase, followed by a steady, slower growth rate until equilibrium is reached. The near-parallel evolution of the curves across piers confirms the absence of hydrodynamic coupling.

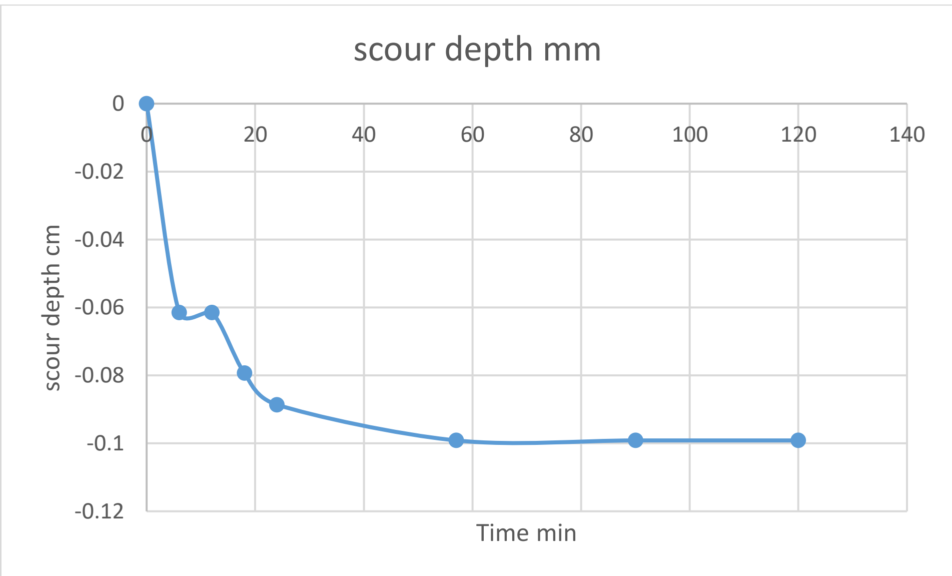


**Figure 4. 15** Development of Scour with Time Z/b=100

### 4.8 Discussion of Results of model's Z/b=1 to Z/b =25

In this study the numerical investigation in local scour around forward-facing triangular pier groups across a range of spacing ratios (Z/b = 1.0, 3.5, 8.45, 15, and 25) reveals a consistent and physically interpretable transition in scour mechanisms, magnitude, and morphology.

At the smallest spacing (Z/b = 1.0), the configuration behaves as a single, compound hydraulic obstacle. the front pier directly obstructs the flow, generating a strong horseshoe vortex at its base and forcing high-velocity flow working like jets through the narrow side gaps. These jets intensify shear stresses on the bed and drive directly into the rear piers' approach zones, producing severe wake turbulence and merged scour holes. The result is a deep, continuous basin with maximum scour depths exceeding 100 mm at the front pier (apex pier) and only slightly less at the rears.

As spacing increases to Z/b = 3.5, contraction effects persist but are less extreme. The front pier still dominates, but the wider gaps allow partial dissipation of the side flow before reaching the rear piers, reducing their scour depths to around 78–81 mm. The scour holes are partially merged, connected by shallower interactions between the scour holes, indicating reduced but still significant hydraulic interaction.

In the transitional case of Z/b = 8.45, the additional separation further reduces wake vortices overlap, enabling more substantial flow recovery between piers. High-velocity regions become localized, and scour holes around each pier are noticeably more separated. Rear-pier scour depths drop further (to ~69 mm), while the front pier (apex) experiences its lowest recorded depth (~88 mm) due to the combination of reduced contraction and partial energy dissipation upstream.

At Z/b = 15, the piers approach hydrodynamic independence. The front pier still receives direct high-energy attack, but the rear piers operate largely under their own local approach flows. Scour holes are fully separated, with depths of ~93 mm at the front pier and ~78–81 mm at the rears. Interaction risk is minimal, and scour morphology is subjected by local vortex systems rather than compound group effects.

In the widest spacing, Z/b = 25, complete hydrodynamic isolation is achieved. Each pier generates its own stagnation zone, horseshoe vortex, and wake, without measurable interference from others. Interestingly, one rear pier surpasses the apex in scour depth (~100.4 mm vs. 96 mm), likely due to minor asymmetries in approach flow distribution. Scour holes are fully independent, steep-walled, and symmetric, confirming the dominance of local conditions. **Although this deference can be neglected ant attribute it as numerical an accuracy due to mesh size that used.**

The comparative trend shows that tight spacing magnifies compound scour risk, transitional spacing reduces interaction effects substantially, and wide spacing eliminates interaction entirely. However, maximum scour depths at isolated piers can still be high, emphasizing the need for targeted protection even when interference is absent.

### 4.9 Comprehensive Evaluation of Hydraulic Effects, Scour Morphology, and Stability Risk

The combined analysis of scour parameters and structural risk across different spacing ratios (Z/b) provides a comprehensive understanding of how geometric configuration influences hydrodynamic behavior, scour morphology, and potential foundation vulnerability. The interaction between the piers' wakes, the contraction of flow through inter-pier gaps, and the ability of the flow to recover flow field momentum before encountering subsequent piers all determine both the depth and distribution of scour holes. At tight spacing ratios ($Z/b \leq 3.5$), hydraulic interaction is intense. The side gaps between the front and rear piers act as high-energy contraction corridors, forcing water into accelerated like a jet that impact the rear piers before the wake can dissipate. This generates large-scale vortex coupling, resulting in fully or partially merged scour holes and significant depths at all piers. Structurally, this scenario carries high to very high failure probability, as group stability is compromised by the loss of sediment around multiple foundations simultaneously. In the transitional spacing range ($Z/b \approx 8.45$–15), the flow begins to regain its structure between piers. Contraction effects weaken, and the wakes overlap less with downstream approach zones. This results in separated scour holes with reduced rear-pier depths while the front pier remains the most exposed to direct attack. Structural risk drops to medium or low, as scour is localized and no longer threatens the group as a single entity. At wide spacing

(Z/b ≥ 25), hydraulic independence is achieved. Each pier generates its own horseshoe vortex and scours hole without interference from others. While maximum depths can still be substantial, risk becomes very low and highly localized. This allows for targeted pier-specific scour protection rather than full-group armoring.

The data in Table 4.9 clearly show that rear-pier scour depths drop sharply when moving from tight spacing (1.0, 3.5) to transitional spacing (8.45, 15), due to the dissipation of jet momentum and reduced vortex overlap. The apex pier consistently records higher depths than the rears, except at Z/b = 25 where one rear pier exceeds it, illustrating the effect of local velocity bias when interaction is absent.

**Table 4. 1** Hydraulic and Scour Parameters for Each Z/b**.**

| Z/b Ratio | Front (mm) | Rear Left (mm) | Rear Right (mm) | Interaction | Morphology |
|---|---|---|---|---|---|
| 1.0 | 100.5 | 94.0 | 97.0 | Fully merged | Single deep basin |
| 3.5 | 92.2 | 78.0 | 81.1 | Partially merged | Deep central + connected |
| 8.45 | 88.0 | 69.7 | 69.3 | Shallow trough links | Separated bowls |
| 15 | 92.8 | 80.9 | 77.9 | Minimal interaction | Fully separated bowls |
| 25 | 96.0 | 100.4 | 92.0 | No interaction | Independent bowls |

Table 4.2 reinforces the link between spacing and structural safety: as Z/b increases, interaction risk declines, stability improves, and the likelihood of simultaneous multi-pier foundation failure falls dramatically. This transition is particularly steep between Z/b = 3.5 and 8.45, marking the shift from a compound scour regime to a localized scour regime.

**Table 4. 2** Structural Risk Assessment by Z/b

| Z/b Ratio | Interaction Risk | Structural Stability | Failure Probability |
|---|---|---|---|
| 1.0 | Very High | Low | High |
| 3.5 | High | Moderate-Low | Moderate-High |
| 8.45 | Medium | Moderate-High | Moderate |
| 15 | Low | High | Low |
| 25 | Very Low | Very High | Very Low |

## 4.9 Summary Discussion of Model Spacing and Recommendations

Table 3 shows that reducing pier spacing increases hydraulic interaction and scour risk, while wider spacing enhances flow stability and reduces scour. In Model 1 (Z/b = 1.0), the very short gap causes severe vortex overlap, merged scour holes, and high risk at all piers, making it unsuitable except under strict spatial constraints. Model 2 (Z/b = 3.5) shows some improvement but still has notable rear-pier scour. Model 3 (Z/b = 8.45), with a 45° attack angle, produces the most severe rear-pier scour and is structurally the least safe, though useful for research calibration. Model 4 (Z/b = 15.0) reduces interaction significantly, with scour patterns approaching isolated-pier behavior, making it an acceptable practical choice. Model 5 (Z/b = 25.0) offers the most stable flow, minimal scour depths, and independent pier behavior, making it the safest option when space allows.

This progression confirms that increasing Z/b shifts the system from a high-risk, compound-scour regime to a low-risk, isolated-pier regime, guiding optimal design choices.

**Table 4. 3** Summary of Model Characteristics, Expected Results, and Design Recommendations

| Model | Z/b Ratio | Z (cm) | Key Hydraulic Features | Expected Results | Design Recommendation |
|---|---|---|---|---|---|
| 1 | 1.00 | 4.0 | Shortest spacing; strong vortex overlap | Very strong pier–pier interaction; relatively deep scour at both front and rear piers | Not recommended unless constrained by severe spatial limitations |
| 2 | 3.5 | 14.0 | Small spacing; beginning of overlap reduction | Noticeable interaction remains; medium to high scour at rear pier | Not ideal, but preferable to Z/b = 1 |
| 3 | 8.45 | 33.8 | 45° attack angle (critical) | Maximum scour at rear pier; peak horseshoe vortex effect | Structurally least safe, but ideal for comparative experimental research |
| 4 | 15.0 | 60.0 | Adequate spacing; gradual interaction reduction | Interaction significantly reduced; scour behavior approaching that of isolated pier | Acceptable design choice without protective measures |
| 5 | 25.0 | 100.0 | Very wide spacing; more stable flow | Piers behave almost as isolated; minimal scour depths observed | Best structural option if space permits |

## 4.10 Analytical Discussion of Model Spacing, Expected Performance, and Design Recommendations

The comparative evaluation of the five studied configurations, summarized in Table 4.3, highlights the clear influence of the spacing ratio (Z/b) and the corresponding physical separation distance (Z) on the hydraulic behavior and scour development within forward-facing triangular pier groups.

In the tightest spacing scenario (Model 1, Z/b = 1.0, Z = 4.0 cm), the extremely short inter-pier distance promotes severe hydraulic interaction. The contraction of flow through the narrow side gaps produces high-velocity jets that directly energize the rear piers, while the wakes merge almost immediately downstream of the apex. This results in fully merged scour holes, with relatively deep excavation at both the front and rear piers. Such a configuration is generally not recommended except under unavoidable spatial constraints, as it poses a high risk to group stability.

Model 2 (Z/b = 3.5, Z = 14.0 cm) exhibits a moderate improvement. Although the onset of reduced vortex overlap is observed, substantial interaction still exists between the piers. The rear piers remain vulnerable to medium-to-high scour depths due to residual turbulence transfer from the apex pier. This arrangement is more favorable than Model 1 but still not optimal for long-term structural safety without significant protective measures.

The critical spacing case (Model 3, Z/b = 8.45, Z = 33.8 cm) introduces a unique hydrodynamic condition, with a 45° attack angle amplifying the horseshoe vortex strength and shifting the zone of maximum scour to one of the rear piers. This creates an asymmetric risk profile, where the rear pier facing the dominant flow path becomes the most exposed. Structurally, this is the least safe configuration in the series; however, its pronounced scour patterns make it valuable for controlled experimental studies and calibration of predictive models.

At larger spacing (Model 4, Z/b = 15.0, Z = 60.0 cm), the hydraulic interaction between piers decreases significantly. The apex pier continues to receive direct flow impact, but the rear piers begin to behave as partially isolated structures, with scour depths approaching those expected for single-pier cases. This configuration offers a balanced design option, minimizing interaction effects while keeping the pier group relatively compact.

Finally, the widest spacing (Model 5, Z/b = 25.0, Z = 100.0 cm) achieves near-complete hydraulic independence between piers. The flow between structures is more stable, wakes are fully dissipated before encountering other piers, and scour depths are the lowest observed in the study. Each pier acts independently, allowing for targeted protective measures and offering the best structural safety margin when space availability is not a limiting factor.

From a design perspective, the progression from Model 1 to Model 5 demonstrates that increasing Z/b gradually transforms the scour regime from a high-risk, group-interaction system to a low-risk, pier-isolated condition. This underscores the importance of considering spacing as a primary design parameter, alongside hydraulic loading, sediment characteristics, and protection strategy selection.

# CHAPTER 5
# CONCLUSIONS AND RECOMMENDATION

## 5.1 Introduction

This chapter synthesizes the outcomes of the numerical simulations carried out to examine local scour around forward-facing triangular pier groups with varying spacing ratios (Z/b). By using a calibrated FLOW-3D model, the study explored how changes in spacing influence the hydrodynamic interactions between piers, the resulting scour morphology, and the temporal development of scour depth. The results are drawn from comprehensive analyses of velocity fields, two- and three-dimensional bed profiles, and scour evolution over time. These findings are interpreted to provide both a scientific understanding of the scour mechanisms in grouped pier arrangements and practical guidance for engineering design and protection strategies.

## 5.2 Conclusions

The investigation has demonstrated that pier spacing plays a decisive role in determining both the severity and the spatial distribution of local scour. In tightly spaced arrangements, such as $Z/b \leq 3.5$, the hydraulic behavior of the group is dominated by strong contraction effects and wake interactions. The apex pier generates intense horseshoe vortices, and the narrow gaps channel high-energy jets directly toward the rear piers. This interaction leads to fully or partially merged scour holes, with depths at the rear piers approaching those at the apex.

When the spacing is increased to intermediate values, particularly in the range of $Z/b \approx 8.45–15$, the flow has more opportunity to recover between piers. The wakes lose some of their energy before reaching downstream piers, resulting in scour holes that are more distinct and less deep at the rears. The apex still tends to exhibit the largest scour depth due to direct impact from the oncoming flow, but the reduction in rear-pier scour is significant, and the risk of simultaneous undermining across the group is much lower.

At the widest spacing, represented by Z/b = 25, the piers behave hydrodynamically as isolated structures. Each pier forms its own horseshoe vortex and wake, and scour development is governed almost entirely by local approach conditions rather than by interactions with other piers. Although scour depths can still be substantial—sometimes even greater at a rear pier due to localized velocity biases—the absence of interaction means the problem is localized to individual foundations rather than affecting the entire group.

A consistent pattern emerged in the temporal evolution of scour across all configurations: the most rapid bed lowering occurred during the initial phase of exposure to the flow, followed by a more gradual approach to equilibrium. This early stage was most intense in the tightly spaced cases, highlighting their vulnerability during short-duration high-flow events such as flood peaks.

Overall, the study confirms that while wide spacing effectively eliminates compound scour interaction, intermediate spacing offers a practical balance between structural compactness and scour risk reduction, and tight spacing requires more aggressive and comprehensive protective measures.

### 5.3 Recommendations

From a design perspective, spacing ratios in the range of Z/b ≈ 8–15 are recommended for multi-pier bridge configurations, as they substantially reduce the transfer of turbulence and high-velocity jets from the apex to the rear piers while avoiding excessively large structural footprints. Where constraints require the use of tighter spacing, the adoption of continuous group-scale scour protection measures—such as riprap aprons, articulated concrete mattresses, or reinforced bed layers—becomes essential to safeguard all piers simultaneously.

In transitional spacing arrangements, targeted protection focused on the apex pier, supplemented by lighter protection for the rears, can achieve effective mitigation with reduced material costs. In contrast, for widely spaced piers where interaction is absent, protection measures can be designed specifically for each pier’s individual scour hole, employing methods such as collars, local riprap placement, or geotextile armoring tailored to the pier's hydraulic exposure.

To maintain long-term safety, regular inspection and monitoring should be integrated into maintenance plans, with particular attention after major flow events. Installing scour monitoring instruments at the most exposed piers can provide early warning of excessive bed lowering. Finally, future research should investigate the effects of skewed approach flows, varying sediment gradations, and the performance of specific countermeasures under a range of hydraulic conditions, to refine and extend the applicability of these findings.

## REFERENCES

Abed, B. S., & Majeed, H. Q. (2020). The behavior of scouring around multiple bridge piers having different shapes. IOP Conference Series: Materials Science and Engineering,

Ahmad, N., Bihs, H., Kamath, A., & Arntsen, Ø. A. (2015). Three-dimensional CFD modeling of wave scour around side-by-side and triangular arrangement of piles with REEF3D. *Procedia engineering*, *116*, 683-690.

Akhlaghi, E., Babarsad, M. S., Derikvand, E., & Abedini, M. (2020). Assessment the effects of different parameters to rate scour around single piers and pile groups: a review. *Archives of Computational Methods in Engineering*, *27*(1), 183-197.

Anand, A., & Beg, M. (2024). Local scour at group of bridge piers founded in gravel bed in staggered arrangement. *Results in Engineering*, *23*, 102608.

Beg, M. (2010). Characteristics of developing scour holes around two piers placed in transverse arrangement. In *Scour and Erosion* (pp. 76-85).

Bettess, R. (2002). A review of predictive methods for general scour. First International Conference on Scour of Foundations, ICSF-1. Texas A&M University, College Station, Texas, USA,

Brethour, J. (2003). Modeling sediment scour. *Flow Science, Santa Fe, NM*.

Chabert, J. (1956). Etude des affouillements autour des piles de ponts. *Rep. Natl. Hydraul Lab., Chatou*.

Chee, R. K. W. (1982). Live-bed scour at bridge piers. *Publication of: Auckland University, New Zealand*(290).

Choi, S. U., & Choi, B. (2016). Prediction of time-dependent local scour around bridge piers. *Water and Environment Journal*, *30*(1-2), 14-21.

Dargahi, B. (1990). Controlling mechanism of local scouring. *Journal of Hydraulic Engineering*, *116*(10), 1197-1214.

Ettema, R. (1980). Scour at bridge piers.

Heidarpour, M., Afzalimehr, H., & Izadinia, E. (2010). Reduction of local scour around bridge pier groups using collars. *International Journal of Sediment Research*, *25*(4), 411-422.

Hirt, C. W., & Nichols, B. D. (1981). Volume of fluid (VOF) method for the dynamics of free boundaries. *Journal of computational physics*, *39*(1), 201-225.

Hoffmans, G. J. (1998). Jet scour in equilibrium phase. *Journal of Hydraulic Engineering*, *124*(4), 430-437.

Jahangirzadeh, A., Basser, H., Akib, S., Karami, H., Naji, S., & Shamshirband, S. (2014). Experimental and numerical investigation of the effect of different shapes of collars on the reduction of scour around a single bridge pier. *PloS one*, *9*(6), e98592.

Jalal, H. K., & Hassan, W. H. (2020). Effect of bridge pier shape on depth of scour. IOP Conference Series: Materials Science and Engineering,

Khaple, S., Hanmaiahgari, P. R., Gaudio, R., & Dey, S. (2017). Interference of an upstream pier on local scour at downstream piers. *Acta Geophysica*, *65*, 29-46.

Kleinhans, M. G., Leuven, J. R., Braat, L., & Baar, A. (2017). Scour holes and ripples occur below the hydraulic smooth to rough transition of movable beds. *Sedimentology*, *64*(5), 1381-1401.

Lu, J.-Y., Hong, J.-H., Su, C.-C., Wang, C.-Y., & Lai, J.-S. (2008). Field measurements and simulation of bridge scour depth variations during floods. *Journal of Hydraulic Engineering*, *134*(6), 810-821.

Maddison, B. (2012). Scour failure of bridges. *Proceedings of the Institution of Civil Engineers-Forensic Engineering*, *165*(1), 39-52.

Malik, R., & Setia, B. (2020). Interference between pier models and its effects on scour depth. *SN Applied Sciences*, *2*, 1-12.

Malik, R., & Setia, B. (2021). Local scour around closely placed bridge piers. *ISH Journal of Hydraulic Engineering*, *27*(4), 396-403.

Melville, B. W., & Coleman, S. E. (2000). *Bridge scour*. Water Resources Publication.

Melville, B. W., & Raudkivi, A. J. (1977). Flow characteristics in local scour at bridge piers. *Journal of Hydraulic Research*, *15*(4), 373-380.

Muzzammil, M., Gangadharaiah, T., & Gupta, A. (2000). Vortex scour mechanism at piers in staggered arrangement. *Journal of the Institution of Engineers. India. Civil Engineering Division*, *81*(DEC), 138-144.

Niedoroda, A., & Dalton, C. (1982). A review of the fluid mechanics of ocean scour. *Ocean Engineering*, *9*(2), 159-170.

Olsen, N. R., & Melaaen, M. C. (1993). Three-dimensional calculation of scour around cylinders. *Journal of Hydraulic Engineering*, *119*(9), 1048-1054.

Pagán-Ortiz, J. E. (2002). Impact of the federal highway administration's scour evaluation program in the united states of north america's highway bridges. First International Conference on Scour of Foundations. November 17-20, 2002, College Station, USA,

Sang, L., Wang, J., Cheng, T., Hou, Z., & Sui, J. (2022). Local scour around tandem double piers under an ice cover. *Water*, *14*(7), 1168.

Tan, J.-S., Elbaz, K., Wang, Z.-F., Shen, J. S., & Chen, J. (2020). Lessons learnt from bridge collapse: A view of sustainable management. *Sustainability*, *12*(3), 1205.

Unger, J., & Hager, W. (2005). The mean characteristics of horseshoe vortex at a cylindrical pier: M. Muzzammil and T. Gangadhariah, Journal of Hydraulic Research, Volume 41, 2003, Issue 3, pp. 285-297. *Journal of Hydraulic Research*, *43*(5), 584-587.

Vijayasree, B., Eldho, T., Mazumder, B., & Ahmad, N. (2019). Influence of bridge pier shape on flow field and scour geometry. *International Journal of River Basin Management*, *17*(1), 109-129.

Wang, C., Liang, F., & Yu, X. (2017). Experimental and numerical investigations on the performance of sacrificial piles in reducing local scour around pile groups. *Natural Hazards*, *85*(3), 1417-1435.

Wang, C., Yu, X., & Liang, F. (2017). A review of bridge scour: mechanism, estimation, monitoring and countermeasures. *Natural Hazards*, *87*, 1881-1906.

Zhang, G., Liu, Y., Liu, J., Lan, S., & Yang, J. (2022). Causes and statistical characteristics of bridge failures: A review. *Journal of traffic and transportation engineering (English edition)*, *9*(3), 388-406.

Zordan, J., Juez, C., Schleiss, A. J., & Franca, M. J. (2018). Entrainment, transport and deposition of sediment by saline gravity currents. *Advances in Water Resources*, *115*, 17-32.